INTERNSHIP REPORT

3D SUPRA-REGIONAL COASTAL GROUNDWATER MODEL: A CASE OF JAVA ISLAND

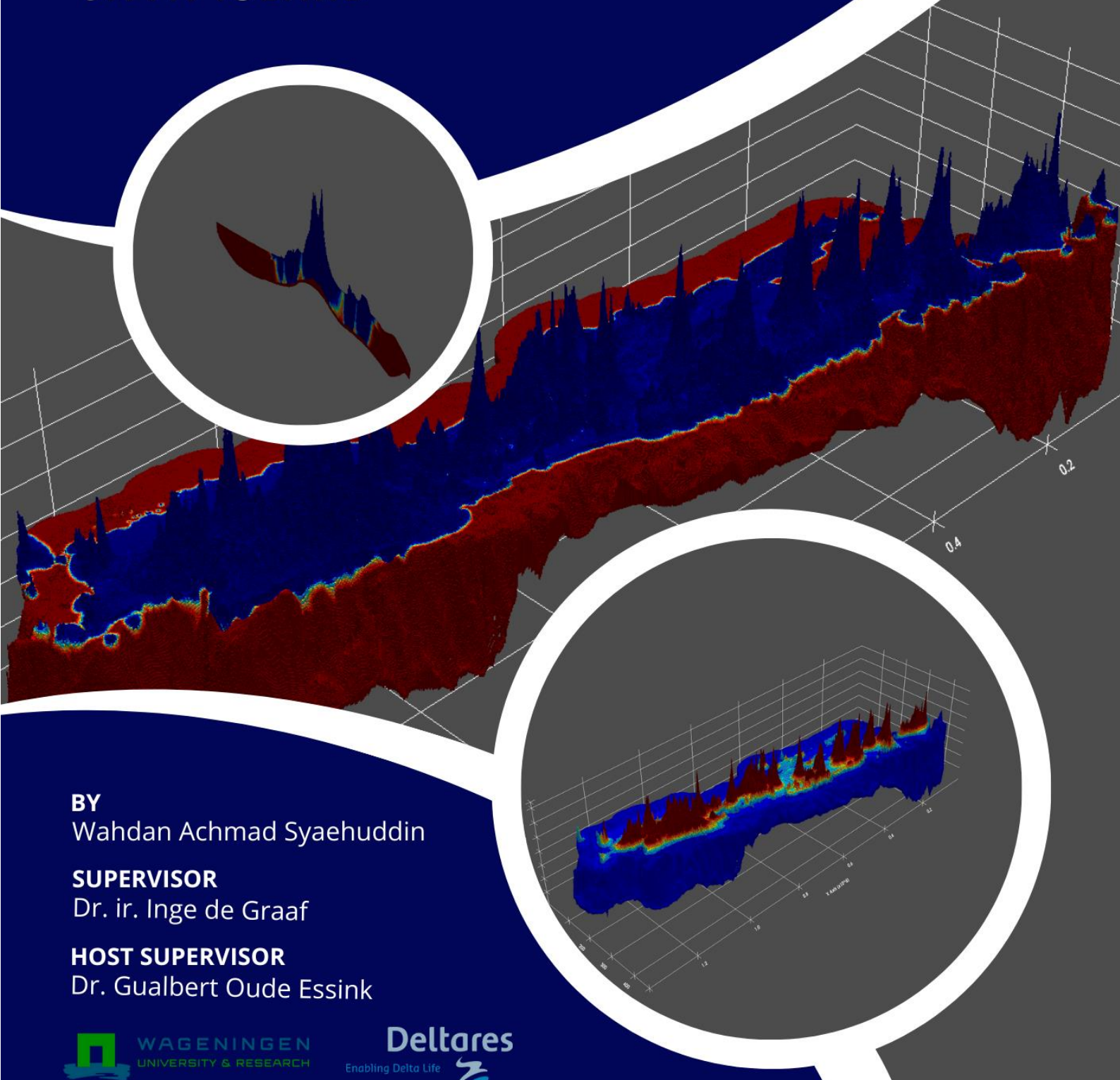

BY
Wahdan Achmad Syaehuddin

SUPERVISOR
Dr. ir. Inge de Graaf

HOST SUPERVISOR
Dr. Gualbert Oude Essink

WAGENINGEN
UNIVERSITY & RESEARCH

Deltares
Enabling Delta Life

Table of Contents

List of Figure

List of Tables

1. Introduction

1.1 Background

Java Island is widely recognized as the most densely populated region in Indonesia. Approximately 70% of Indonesia's urban population is concentrated on this island, which has a total of 118 cities, with 63 of them situated along the coastal regions (Badan Pusat Statistik, 2023; Handayani & Kumalasari, 2015). In total, around 75 million people live along the northern and southern coasts of Java (Badan Pusat Statistik, 2023). Three of the most important places on this island are located in the coastal region which is Jakarta, Semarang, and Surabaya which have become central for industrial and economic activity in Indonesia (Handayani & Kumalasari, 2015).

The coastal region situated on Java Island has a vulnerability to several natural hazards and disasters. The island's northern coast is susceptible to subsidence and coastal flooding, whereas the southern coast has the potential to face tsunamis (Horspool et al., 2014; Supendi et al., 2023; Willemsen et al., 2019). Furthermore, the salinization process occurs naturally in this region because of its closeness to the sea. This problem will likely get worse in the future due to climate change which will influence the precipitation pattern and sea level rise (Intergovernmental Panel on Climate Change (IPCC), 2022). A decrease in precipitation will have an impact on the decline of groundwater recharge that is needed for the replenishment of groundwater storage. Sea level rise also will make the coastal area more vulnerable to coastal inundation which will increase the rate of salinization of the coastal groundwater system (Purnama & Marfai, 2011).

Groundwater is one of the most important resources in Indonesia. Groundwater makes up about 15% of total water withdrawals in Indonesia which is used for drinking water alone (Badan Pusat Statistik, 2023; USAID, 2021). According to the Asian Development Bank(ADB, 2016), around 64% of the urban population and 69% of the rural population have access to an adequate water supply. It is noteworthy that a significant portion of this water supply, almost half, is sourced from dug wells (shallow groundwater) and bored wells (deep groundwater). Only 30% of this clean water supply is provided by water supply companies, with the rest of it depending on community/local water systems, or most of it is private systems (ADB, 2016). Thus, the exact number of groundwater extractions is unknown but likely more than the official number. This demand will likely increase as increasing of population and industrial growth and give more stress to the water system.

The negative impact resulting from excessive groundwater extraction has become apparent in several locations of Java, especially in the northern coastal area. Jakarta has become famous as a sinking city dealing with the issue of land subsidence. This area has a sinking rate of 6 cm/year as a result of excessive extraction of groundwater, as documented by Widodo et al. (2019) and Bott et al. (2021). In the region of Semarang, the extraction of groundwater for industrial and agricultural purposes has resulted in the occurrence of land subsidence. This phenomenon has been observed at a rate of around 10 cm per year (Bott et al., 2021). Additionally, several areas in the Semarang-Demak coastal area have experienced recurrent tidal flooding throughout the year (Andreas et al., 2017; Putranto & Rüde, 2016).

To overcome the challenge faced by groundwater systems in Java, certain mitigation and groundwater management will be needed. One of the ways to help this is by modeling the groundwater system in the coastal Java area to know the effect of sea level rise, tidal inundation, and anthropogenic effects like groundwater abstraction. Through the Global Coastal Groundwater Model (GCGM) project, Deltares and Utrecht University collaborated in developing this GCGM (iMOD-WQ, iMOD-Python) to understand the effects mentioned above.

1.2 Variable-Density Groundwater Flow

Groundwater flow is influenced by hydraulic gradients, but in certain circumstances, the density of the fluid is important in controlling the groundwater flow. In the coastal aquifer, for example, the density of the saline water is present, and the value is higher than the density of the fresh water. The difference in density and value will result in groundwater flowing down from water with high salinity to lower salinity. Furthermore, this process will create the interface between seawater and freshwater and create a mixing area.

1.3 Groundwater Quality

The mixing between the different densities of the fluid in the groundwater system will create several different solute densities and concentrations. In this section, the type of fresh, brackish, and saline water needs to be determined.

1.4 iMOD-WQ and Parallel Computing

iMOD-WQ is programming code for a coupled salt transport-groundwater flow model developed by Deltares in collaboration with Utrecht University. This code integrates SEAWAT and MT3DMS code developed by USGS.

1.5 Research Objectives

The primary objective of this study is to simulate the groundwater system in Java Island, Indonesia by building and applying a 3D variable-density groundwater model and coupled salt transport model.

The specific research objectives are:

1. Paleo-Reconstruction of Groundwater System in Java Island, Indonesia.
2. Feature Analysis: Analyze the effect of the river package on the system and also the effect of recharge (homogenous and spatial variability). On the numerical side, the effect of the timestep (DT0) value will be analyzed.
3. Effect of storm surge on the groundwater system.
4. Effect of anthropogenic on the groundwater system.

1.6 Research Questions

1. How is the change in Java's groundwater system in the past 30ka?
2. What is the impact of the improved feature in the model on the result of the model?
3. What is the effect of storm surge, sea level rise, and anthropogenic activities on the groundwater system?

2. Data and Methodology

2.1 Data

Several data are collected as input for the construction of 3D GCGM of Java Island. The overview of the data used in this research can be seen in Table 1. The following section will give more description of each dataset.

Table 1. Summary of data used in this research.

Data	Temporal	Spatially	Reference
Last Glacial Maximum and Holocene Sea Level	Yes	No	Kim et al. (2023); Sathiamurthy & Voris (2006)
Paleo-Precipitation	Yes	Yes	Beyer et al. (2020)
Recharge	Yes	Yes	Sutanudjaja et al. (2018)
Groundwater Abstraction	Yes	Yes	Sutanudjaja et al. (2018)
GAIA Global River Database	No	Yes	Andreadis et al. (2013)
Thickness of Unconsolidated Coastal Aquifers	No	Yes	Zamrsky et al. (2018)
GEBCO: Global Topography and Bathymetry	No	Yes	(Weatherall et al., 2015)
Average Soil and Sedimentary Deposit Thickness	No	Yes	(Pelletier et al., 2016)

2.1.1 Bathymetry and DEM

Bathymetry displays the surface elevation of underwater bodies such as seas and lakes and it includes the spatial framework that corresponds to terrestrial topography (Weatherall et al., 2015). In this study, the GEBCO dataset developed by Weatherall et al. (2015) has been used as the top elevation of the model. The resolution of this data is 30 arcsec, which is equivalent to approximately 1x1 km (Weatherall et al., 2015). Figure xx shows the topography of Java Island.

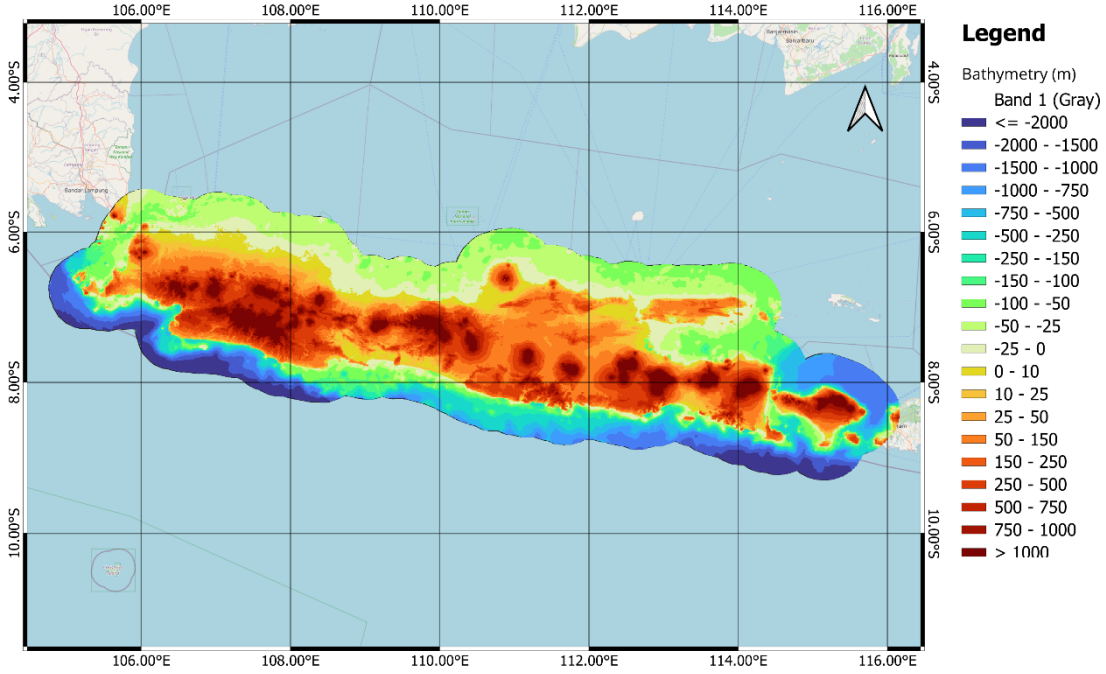

Figure 1. Java Island Bathymetry and DEM

2.1.2 Sea Level Change

The sea level fluctuation is taken from the last 30ka ago the last glacial maximum and Holocene era. The sea level of the last glacial maximum is obtained from Kim et al. (2023) who studied how sea level rise driven migration in the Sundaland area (now Southeast Asia). For the Holocene era, sea level fluctuation data from Sathiamurthy and Voris (2006) had been used. Figure xx illustrates the fluctuation in sea level over the past 30,000 years, showing a significant rise in marine transgression starting approximately 15,000 years ago.

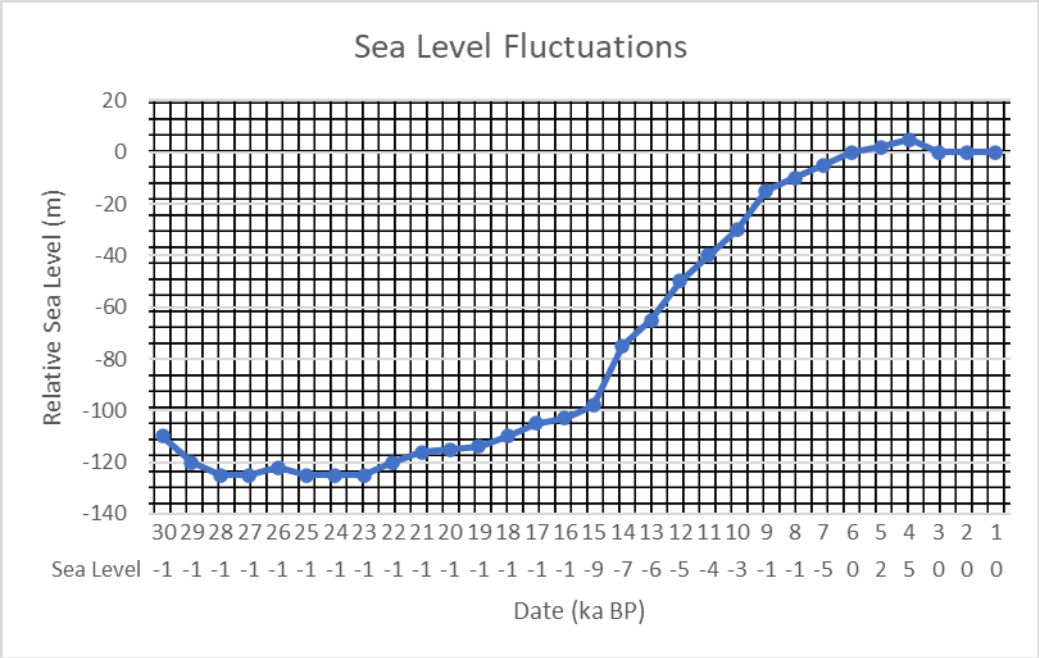

Figure 2. Sea Level Fluctuation in Sunda Shelf for the Last 30ka years ago

2.1.3 Paleo-Precipitation and Recharge

The recharge package input for the paleo reconstruction was using paleo precipitation data due to the unavailability of paleo recharge data for the last glacial maximum and Holocene era. Paleo precipitation data is acquired from Beyer et al. (2020). For the paleo reconstruction scenario and present scenarios such as groundwater abstraction and tidal inundation scenario, recharge with spatial variability value has been used instead of one recharge value for all Java areas. In addition, the recharge input for paleo reconstruction also has temporal variability for every 1000 years. The paleo precipitation data has 0.5° resolution and is already bias-corrected (Beyer et al., 2020). Figure 3 displays the precipitation rate for 30,000 years ago in m/day.

Furthermore, recharge data obtained from the PCR-GLOBWB model (Sutanudjaja et al., 2018) has been used for more present scenarios. The resolution of this data is 5 arcmin, as reported by Sutanudjaja et al. in 2018. Figure 4 displays the average daily recharge rate throughout the period from 1986 to 1995. This study utilizes the average daily recharge rate for the time frame spanning from 1986 to 2015, segmented into intervals of 10 years.

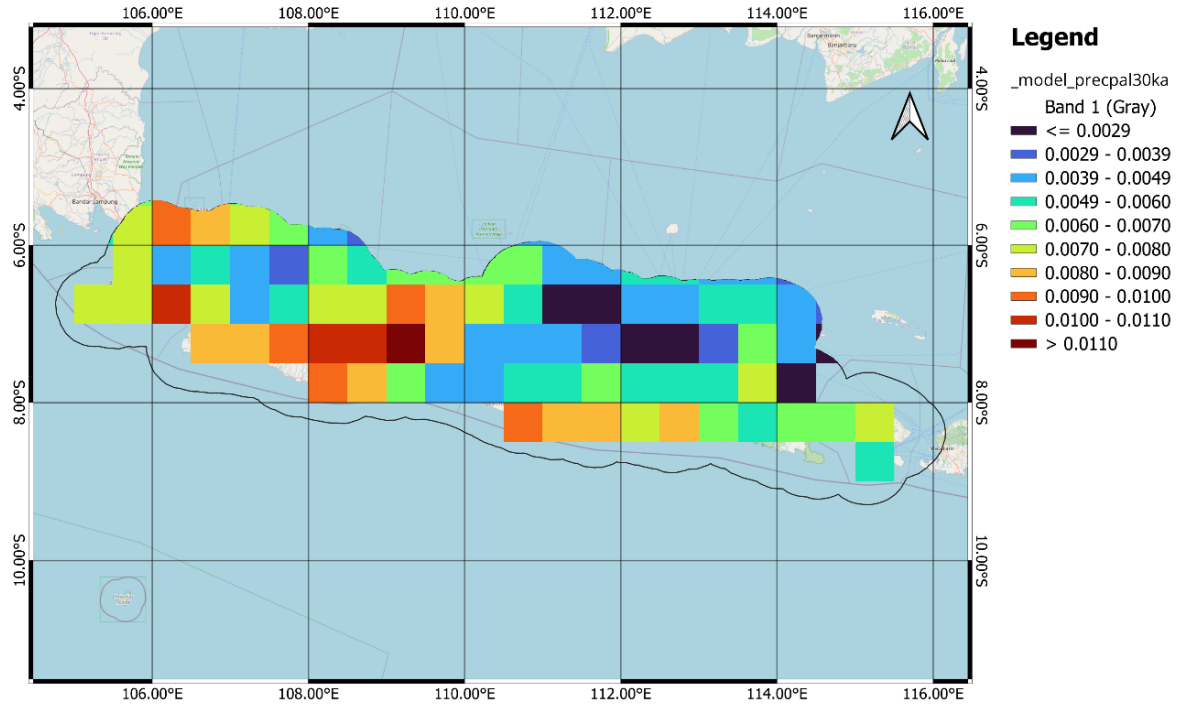

Figure 3. Average paleo-precipitation rate (m/d) for 30ka years ago.

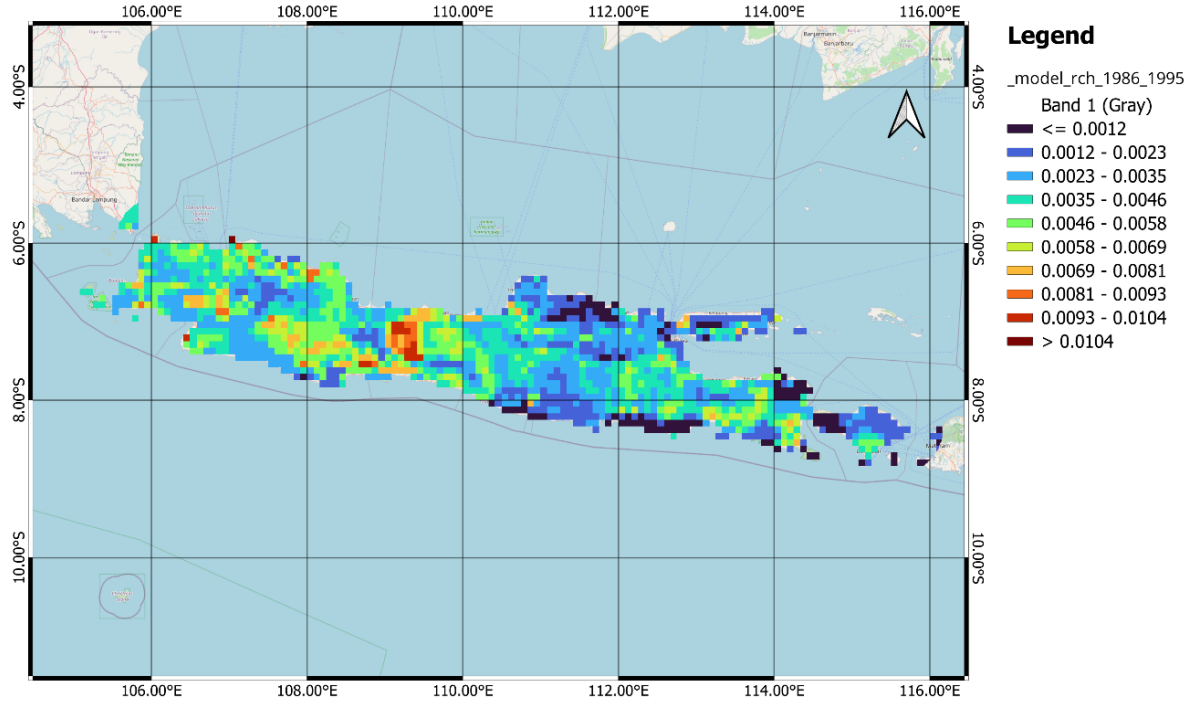

Figure 4. Average recharge rate (m/d) for Java Island for the period of 1986-1995 (Data from PCR-GLOBWB).

2.1.4 Groundwater Abstraction

Groundwater is one of the important water sources in Java Island, especially in coastal urban areas. Thus, it is important to simulate the effect of groundwater abstraction on the status of coastal aquifers. Input data for groundwater abstraction is acquired from the PCR-GLOBWB model (Sutanudjaja et al., 2018). The data shows the spatial variability of the groundwater abstraction in Java (Figure 5).

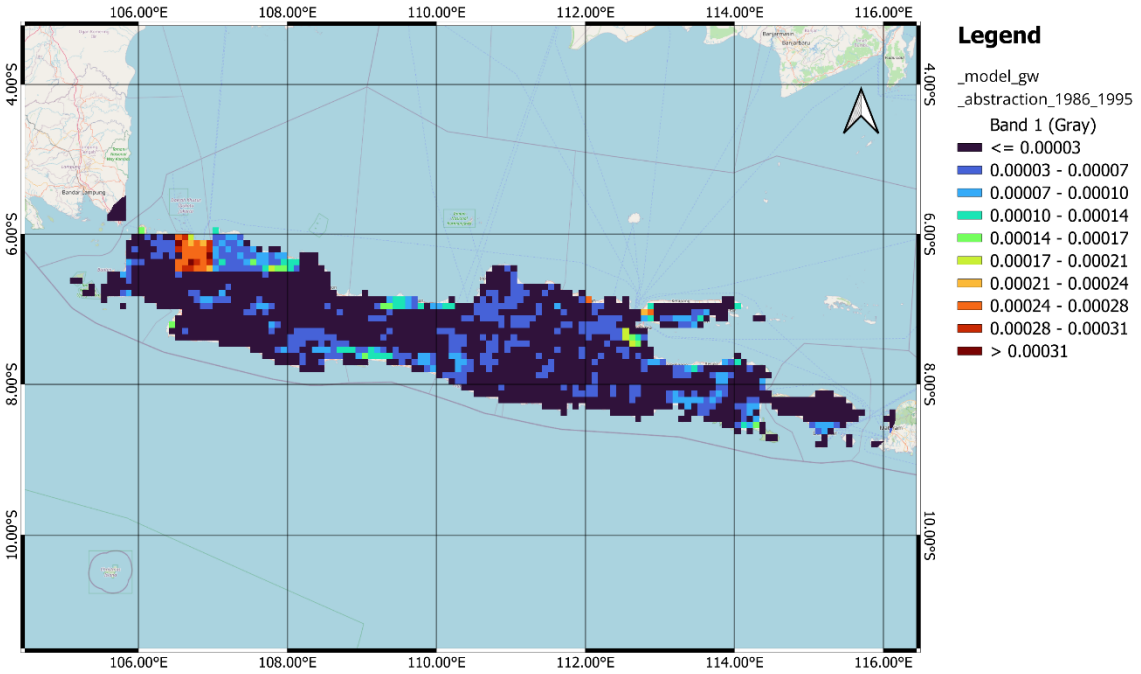

Figure 5. Average daily groundwater abstraction (m/d) for the period 1986-1995.

2.1.5 River

GAIA river network dataset (Andreadis, et al., 2013) is utilized for incorporating rivers into the GCGM model. Beside the river line, this dataset also contains the width and depth of the rivers (Andreadis, et al., 2013). The depth of the rivers and the top elevation of the models are used to determine the stage of the river in the model. The conductance of the model is determined following the equation by Mulder (2018). The conductance value is determined by multiplying the width of the river by 10. This is proven to give a rough estimation of the river conductance (Mulder, 2018).

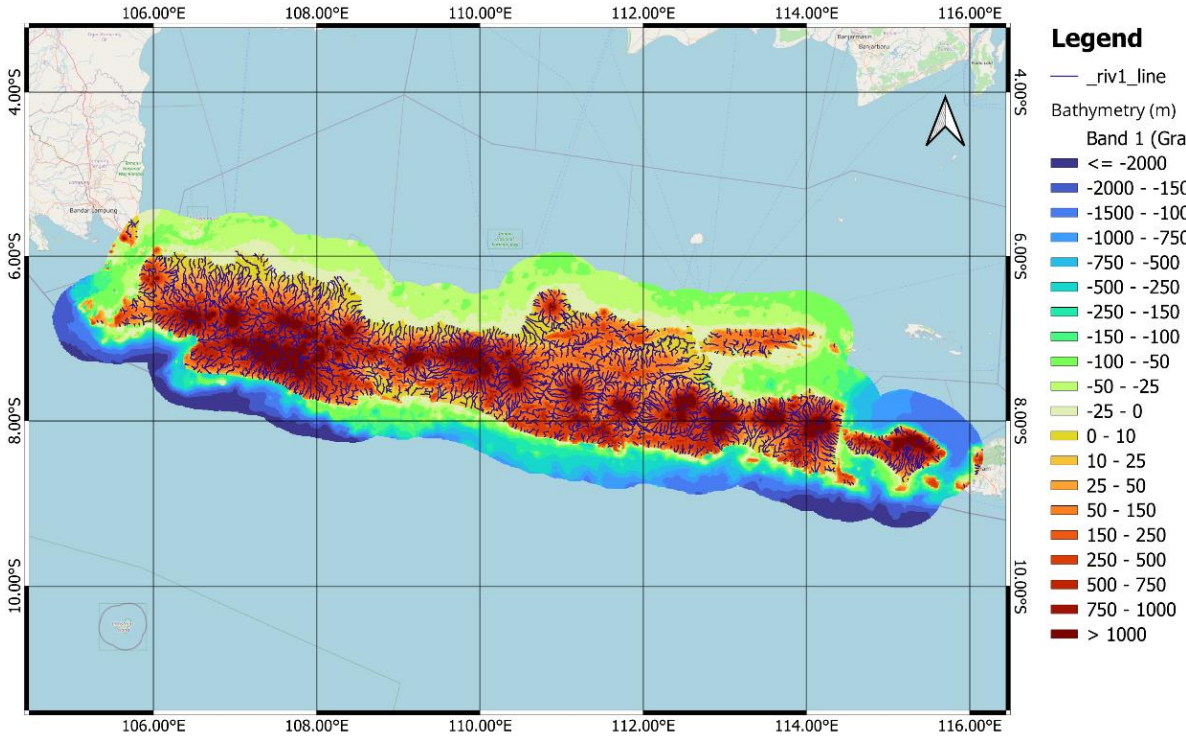

Figure 6. River network of Java Island

2.1.6 Thickness of Unconsolidated Coastal Aquifers

To determine the bottom elevation and thickness of the model, this research uses the data from Zamrsky (2018). The study provides an approach for determining the depth of unconsolidated coastal aquifers by utilizing existing information on the geological structure, surface elevation, and bathymetry of the coastal region. Figure 7 shows the result of the thickness of unconsolidated sediment on Java Island.

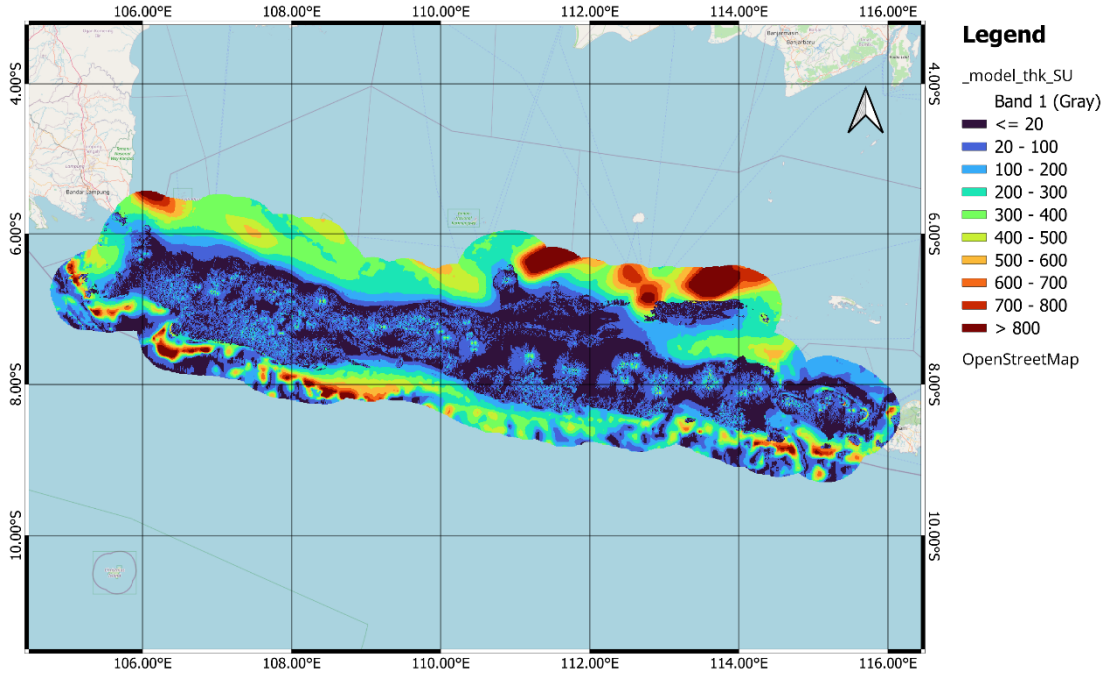

Figure 7. Thickness of unconsolidated sediment

2.1.7 Salinity Classification

One of the objectives of this study is to quantify the groundwater quality in the coastal area of Java. Thus, it is important to determine the classification of the class of water quality, based on water salinity. The salinity classification is based on the USGS classification for TDS values as detailed below:

- Freshwater—less than 1000 mg/l,
- Slightly saline water—from 1000 to 3000 mg/l
- Moderately saline water—from 3000 to 10,000 mg/l
- Highly saline water—from 10,000 to 35,000 mg/l (seawater is 35,000 mg/l)
- Brine—more than 35,000 mg/l

2.2 Methodology

In this research, several steps were taken to understand and apply the 3D GCGM model in the case of Java Island:

1. Three main tools are used to understand the groundwater model which are iMOD-WQ (Verkaik et al., 2021), phyton script (Zamrsky et al., 2022), and floppy python package (Bakker et al., 2016).
2. Local and global data collection for parameters in the GCGM.
3. Model Building with different initial salinity distribution.
4. Running several model scenarios.

5. Analysis of the result.
6. Reporting

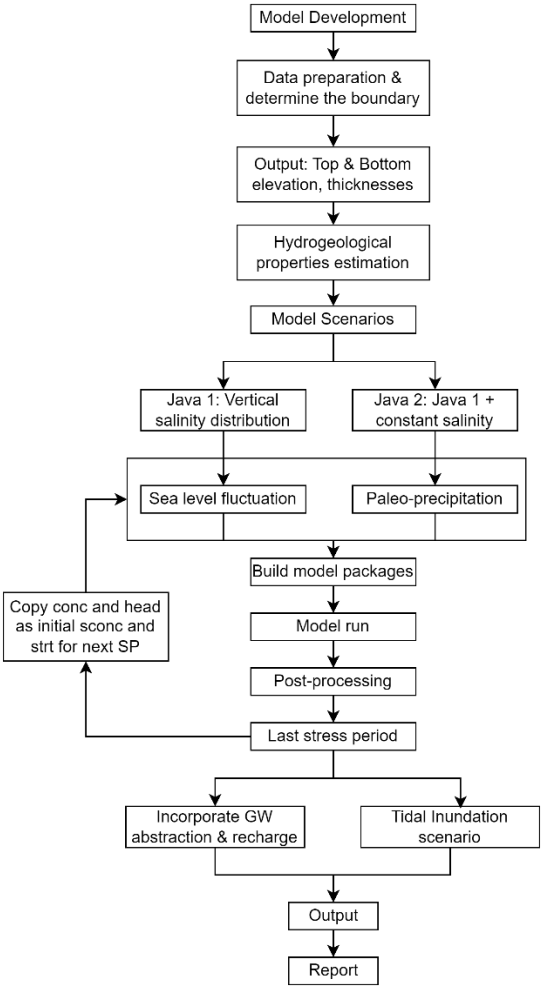

Figure 8. Methodology framework for this research

2.2.1 Numerical Model Setup

A 3D variable-density groundwater flow model coupled with a salt transport model, was constructed using the GCGM toolbox. In this study, the Python FloPy package was utilized to facilitate the input files that later entered the iMOD-WQ model (Verkaik et al., 2021).

The area of interest which include Java Island and Bali cover around 134,077 km² and a grid size of 463 m x 1368 m with 1 x 1 km cell size. The model layer uses using unstructured grid, in this research two different model layers are used which are 14 and 16 layers. The boundary of the model is displayed in Figure 9 below. The distance of the coastal boundary is 50 km from the coastline, and it is done automatically using QGIS software.

Layer property package (LPF) is used to determine the physical properties of the model, especially for horizontal and vertical hydraulic conductivity. This model has been designed as a conceptual model, meaning that it does not utilize local geological layer data and instead relies primarily on global data. For the aquifer, the hydraulic conductivity is set to be homogenous at 10 m/d aquitard is set to be 0.01 m/d, and the sedimentary rocks to be 0.1 m/d. Whether the layer is identified as aquifer or aquitard is based on the top elevation and thickness of the model.

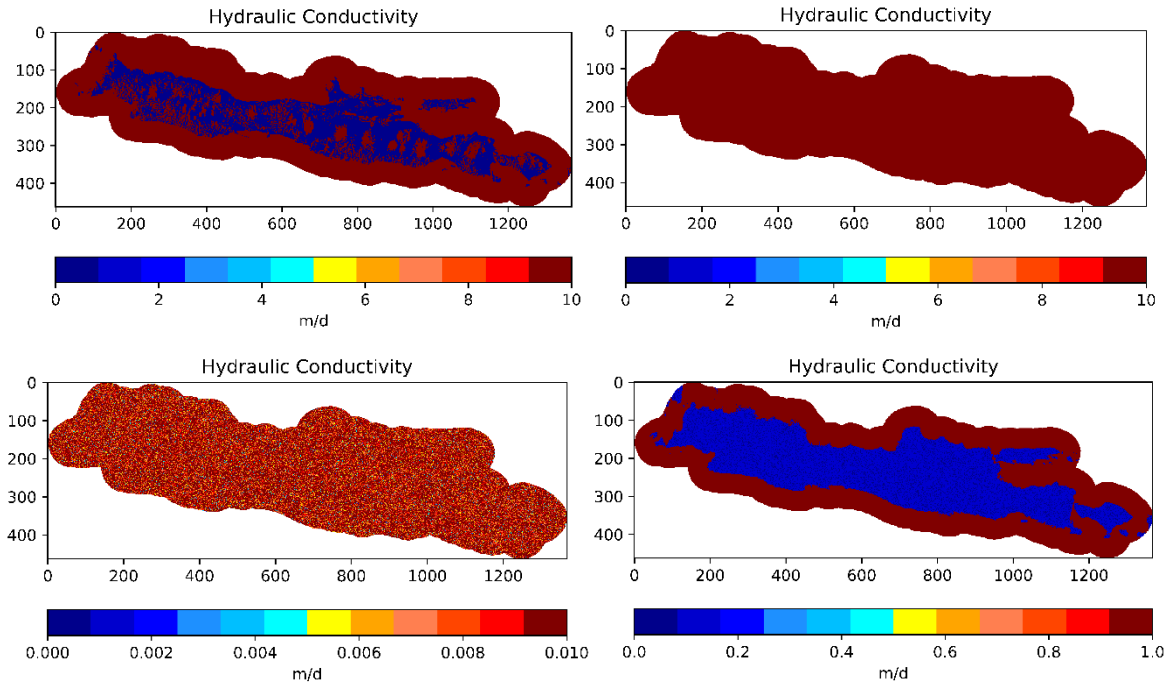

Figure 9. Hydraulic conductivity of the model (1. Upper part: left = 1st layer; right = 2nd layer. 2. Bottom part: left = 4th layer; right = 7th -16th layers).

Figure 10. Model boundary

In the general head boundary package (GHB), some variables are determined in this package. The GHB cells will contain head, conductance, and density. The head values are different for land and offshore boundary. The head for the inland boundary is set to be minimum values between top elevation and a fixed value of 25 m. Offshore, the head is set to be equivalent to the sea level. The conductance for the inland is set to be 0.1 m^2/d while for the coastal areas is set to be 100 m^2/d. In the initial phase of building the model, a higher conductance value for the coastal area is being used, but there is a convergence issue and also there is a weird result salinity value in the coastal area. The density value is set to be 1000 kg/m^3 for freshwater and 1025 kg/m^3 for saline water.

The recharge (RCH) package used paleo precipitation data (Beyer et al., 2020) and recharge rate data (Sutanudjaja et al., 2018) as input depending on the scenario. The recharge is set on the first layer of the model.

The drainage (DRN) package is utilized to determine the location, stage, and conductivity values of the drainage area. The drain is active when there is water above the drainage level, and inactive when there is not. The location of the drainage area is set on the first layer of the model. The stage of the drainage is set to be -0.5 meters below the surface elevation. The conductivity of the drain is 1000 m^2/d.

The input for the river package (RIV) is from the GAIA river network dataset. This dataset contains information such as the depth and width of the river. These two pieces of information are used to determine the river stage and river conductance of the model. The river stage is calculated by summing the surface elevation of the model with the depth of the river. The river bottom is set to be the value of surface elevation. Last, the river conductance is set by multiplying the river width by 10. Figure xx shows the spatial variability of the river conductance.

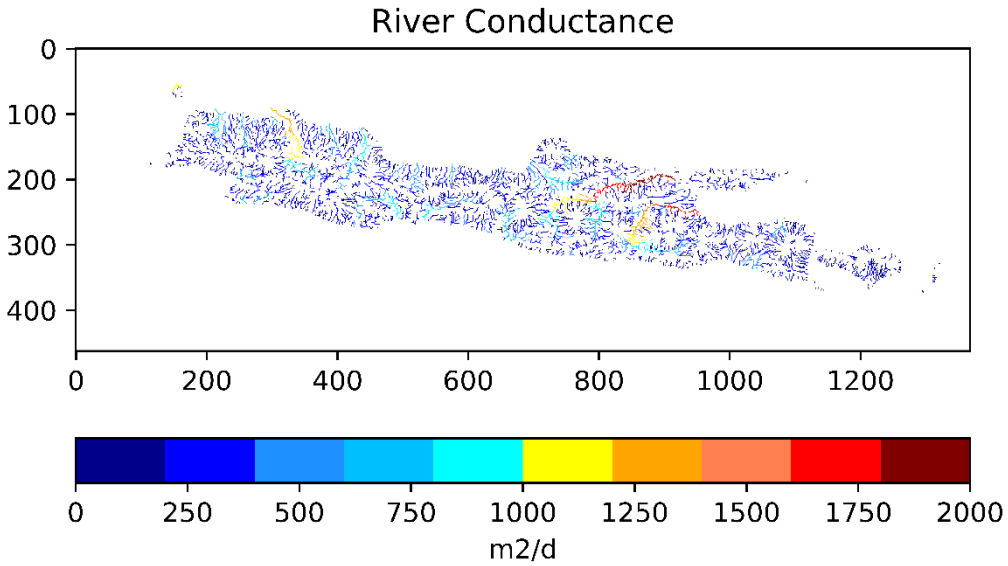

Figure 11. River conductance

Wel package (WEL) is used to implement the groundwater abstraction in the model. The input for this package is the data from PCR-GLOBWB (Sutanudjaja et al., 2018). In the output control package (OC), the head, concentration, and velocity as TECPLOT files are saved. A basic transport package (BTN) is used to set the initial concentration of the model and the stepsize of the model. In one paleo reconstruction scenario, the last layer in the model is set to have constant concentrations throughout the years. This is done by setting the cells in this layer value from 1 to -1. The stepsize that has been used, after several trials and errors of the value, is set to be 3652.5 days or 10 years to make the model run faster. The difference between the results of different stepsize values will be shown in the result and discussion chapter.

Table 2. The parameter is fixed throughout the simulation.

Parameters	Value	Unit
Effective Porosity	0.3	-
Storage Coefficient	0	-
Sea Salinity	33	g TDS/l

Initial Freshwater Salinity	0	g TDS/l
Longitudinal dispersivity	1	m
Horizontal Transversal Dispersivity	0.1	m
Vertical Transversal Dispersivity	0.1	m
Molecular Diffusion Coefficient	0.0000864	m^2/day
Duration of paleo stress period	1000	Year
Cell size	463 x 1368	m

3. Results and Discussion

3.1 Effect of Different DT0 Values

Paleo-reconstruction is time-consuming in terms of running process. Parallel computation is one way to make the running process faster than using one core in the computer. Alas, sometimes for a system with a larger area, the running process could still take a long time. In this research, another option to make the running process faster is identified by modifying the DT0 value. This value determines the initial transport step size within each time step of the flow solution with the default value is 0. If the value is set to zero, the model will utilize the calculated value of DT0, which is determined by the user-specified Courant number in the Advection Package. Determining the DT0 to a certain value will force the system to obey this value, thus the running process is faster.

One of the concerns of forcing the DT0 value is how it affects the distribution of salinity and head at the end of the process. If the change in this value does not have a big impact on salinity and head, it will be useful to use a bigger DT0 value in making paleo-reconstruction.

In this study, eight different DT0 values were used to identify the effect of this change on the output of the model. The first model uses the default value which is 0, and the other models use the value from 100 – 10000. For the testing, the model is run for 100 years. Table 3 shows the different running time processes for the model and the stepsize. A higher DT0 value certainly increases the processing of the model but there is a need for attention with a higher value there is a probability the model will crash. In this case, with the DT0 value set to 5000, the model cannot converge.

Table 3. The runtime and stepsize of the model with different DT0 values

DT0	Runtime	Stepsize
0	8h 55m	6.28
100	1h 18m	6.254
1000	44m 38s	6.406
2000	32m	6.258
3000	31m	6.301
4000	32m	6.37
5000	Model Crash	
10000	Model Crash	

Different DT0 values do not affect the water budget in the model (Figure 12). Figure 12, it can be seen similar values of the water entering and exiting the system majority via recharge and drainage. The concentration and head in the output of the model also don't have a bigger impact due to changes in DT0 value (the majority is still below 10% change). In Figure 13, the percentage of concentration change between models with DT0=0 and DT=100 (a) and DT0=0 and DT0=4000 (b). This scenario is for the lowest and highest DT0 value used in the model without crashing the model.

Based on this parameter alone, it can be concluded that the utilization of a higher DT0 value will be beneficial to increase the speed of the model without too much compensation for the accuracy of the model. Therefore, in this study, a higher DT0 value is employed for the paleo reconstruction to accelerate the model processing.

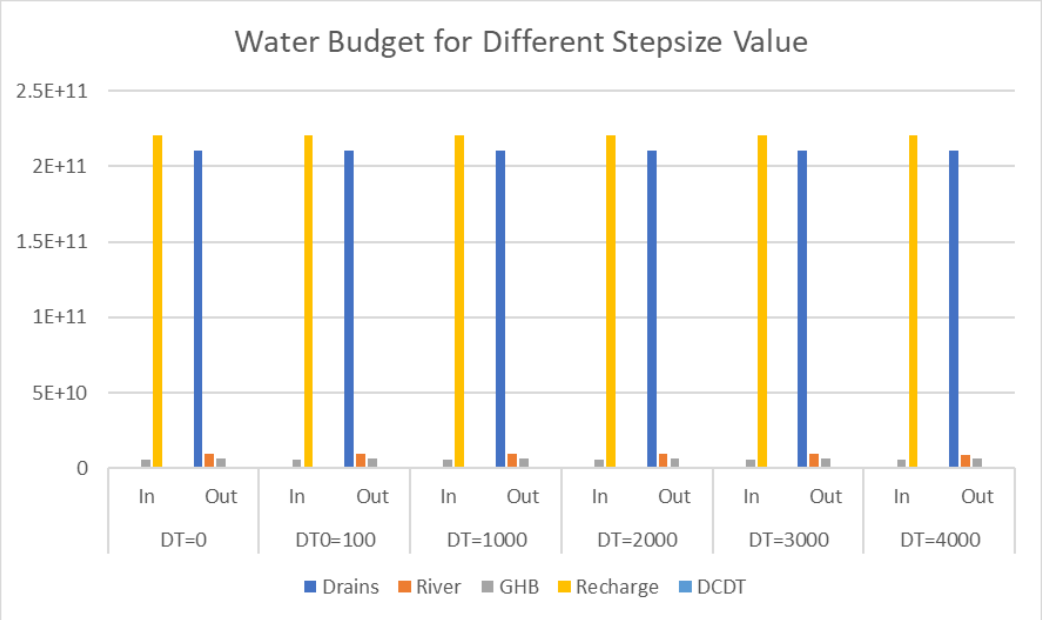

Figure 12. Water budget of different DT0 values

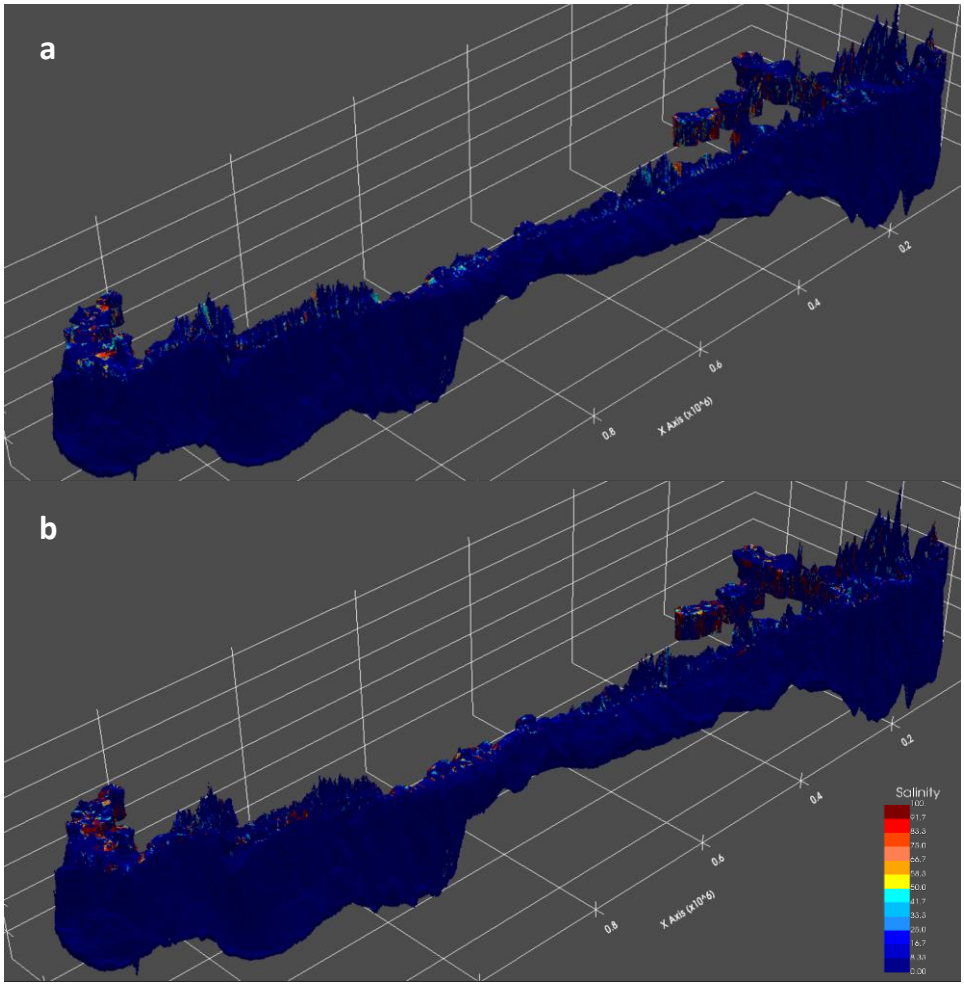

Figure 13. Different concentrations value in percentage between model with DT0 = 0 and DT0 = 100 (a); DT0 = 0 and DT0 = 4000

3.2. Paleo-reconstruction Groundwater System of Java Island

3.2.1 Java 1 Scenario: Vertical Initial Salinity Distribution

The Paleo reconstruction model was made to analyze the effect of sea level fluctuations over 30,000 years ago and how it affects the present groundwater status. This model was also used to create the present salinity distribution model (later applied in groundwater abstraction and tidal inundation scenarios). The Hydrogeological setting for this scenario is shown in Table 4 below.

Table 4. Java 1 Hydrogeological Setting Models

Layer No.	Thickness (%)	Classification	HK mean and standard deviation (m/d)	VK (m/d)
1	5% of SU	Aquifer/Aquitard	Depends on top elevation value	10% HK
2	29% of SU	Aquifer	10 and 0	
3	29% of SU	Aquifer	10 and 0	
4	37% of SU	Aquitard	0.01 and 0.0025	
5	10% of SS	Aquitard	0.1 and 0.02	
6	10% of SS	Aquitard	0.1 and 0.02	
7	10% of SS	Aquitard	0.1 and 0.02	
8	10% of SS	Aquitard	0.1 and 0.02	
9	10% of SS	Aquitard	0.1 and 0.02	
10	10% of SS	Aquitard	0.1 and 0.02	
11	10% of SS	Aquitard	0.1 and 0.02	
12	10% of SS	Aquitard	0.1 and 0.02	
13	10% of SS	Aquitard	0.1 and 0.02	
14	10% of SS	Aquitard	0.1 and 0.02	

This model consists of 14 layers with the top layer consisting of an aquifer and aquitard depending on elevation and the thickness of the layer. The aquifer layers are made homogeneous while the aquitard and sedimentary rocks layer have variability hk values. More elaboration of the model will be given in the second scenario. Since the parameters of the model are not much different the initial salinity distributions only have differences regarding the constant concentration in the last layer of the model.

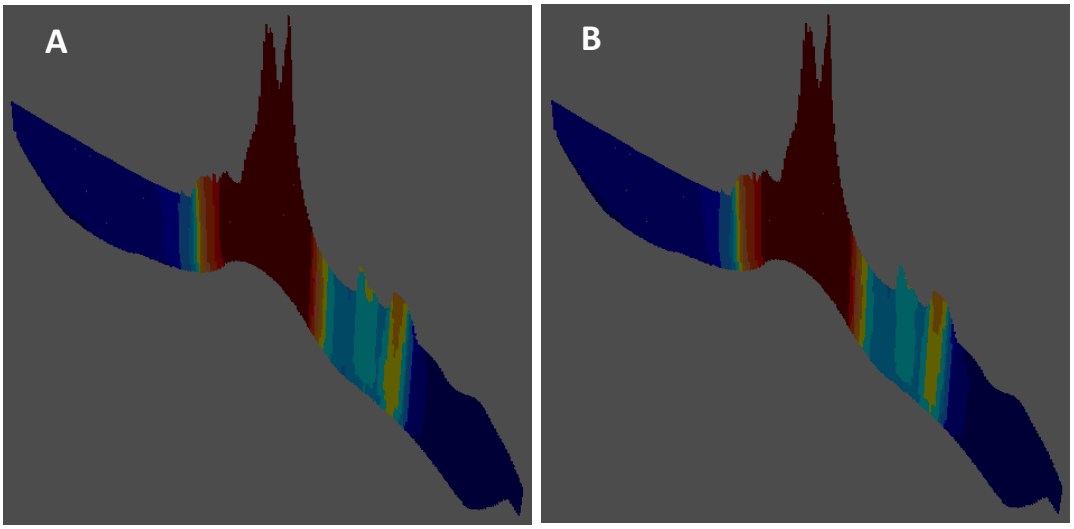

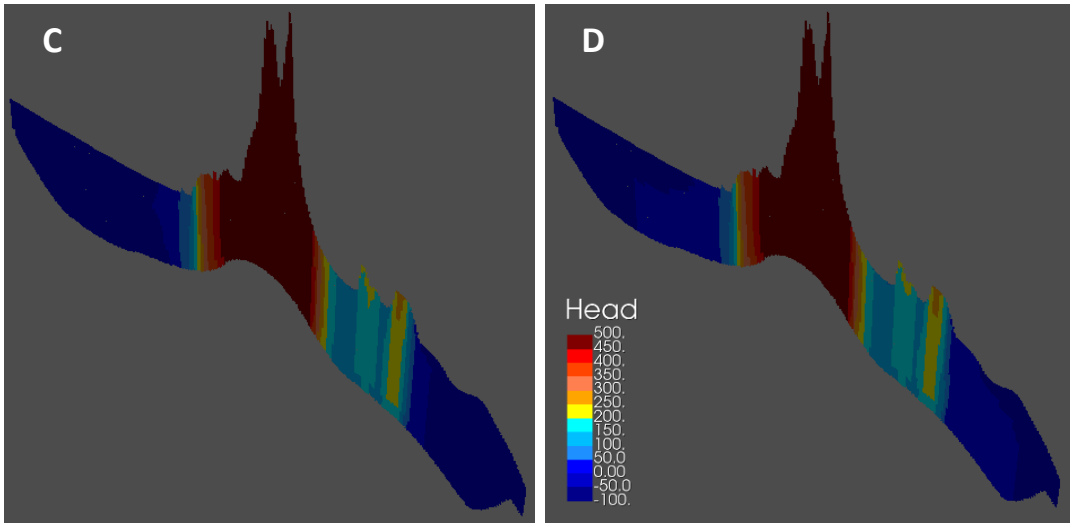

Figure 14. Head profile for BP30000 (A), BP15000 (B), BP08000(C), and BP01000 (D)

Figure 14 displays the change in head profiles throughout the years in paleo reconstruction. The head values are increasing following the increase in sea level rise due to marine transgressions. The north coast of Java experiences a greater impact from sea level change due to its shallower coastal depth compared to the south coast of Java.

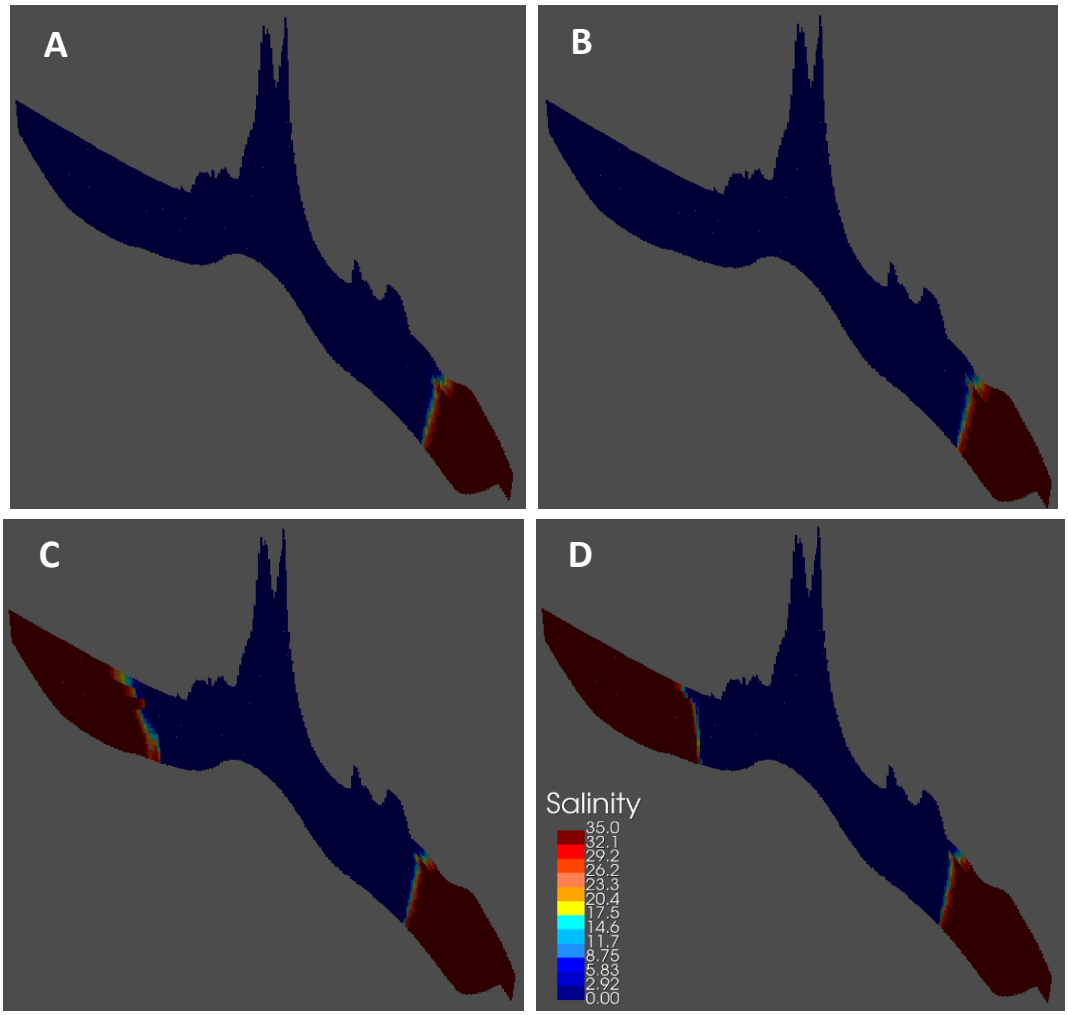

Figure 15. Salinity distribution for BP30000 (A), BP15000 (B), BP08000(C), and BP01000 (D).

3.3.1 Java 2 Scenario: Constant Salinity in the Bottom Layer

The second scenario for the paleo reconstruction is using a similar vertical salinity distribution but adding the constant salinity concentration in the last layer of the model. This objective is to identify the saline water that is present in the inland areas and one of the possible sources is the saline water that was trapped in the past time. This model consists of 16 layers, detailed can be seen in Table 15.

Table 5. Java 2 Hydrogeological Setting Models

Layer No.	Thickness (%)	Classification	HK mean and standard deviation (m/d)	VK (m/d)
1	5% of SU	Aquifer/Aquitard	Depends on top elevation value	10% HK
2	20% of SU	Aquifer	10 and 0	
3	20% of SU	Aquifer	10 and 0	
4	20% of SU	Aquitard	0.01 and 0.0025	
5	20% of SU	Aquifer	10 and 0	
6	15% of SU	Aquitard	0.01 and 0.0025	
7	10% of SS	Aquitard	0.1 and 0.02	
8	10% of SS	Aquitard	0.1 and 0.02	
9	10% of SS	Aquitard	0.1 and 0.02	
10	10% of SS	Aquitard	0.1 and 0.02	
11	10% of SS	Aquitard	0.1 and 0.02	
12	10% of SS	Aquitard	0.1 and 0.02	
13	10% of SS	Aquitard	0.1 and 0.02	
14	10% of SS	Aquitard	0.1 and 0.02	
15	10% of SS	Aquitard	0.1 and 0.02	
16	10% of SS	Aquitard	0.1 and 0.02	

Following Alkurd (2023) suggestion, a river package has been incorporated into the model. The island of Java possesses a substantial river network, which is likely influencing the flow of groundwater through the interplay of the surface and subsurface water systems. A river system can serve as a recharge area or input to the groundwater system when the value of the river head is higher than that of the groundwater head. Conversely, it functions as a drainage area when the elevation of the river head is lower.

A study by Irawan et al. (2015) showed the close connection between surface and groundwater systems in the Ciliwung River Basin (Bogor-Jakarta Area). Based on field observations, Irawan et al. (2015) found that these two systems exhibit similarities in terms of temperature and TDS profile. Therefore, it is crucial to incorporate river networks into groundwater models for Java Island.

Figure 16 shows the water budget for the models with and without the river system. The river package impacts the input of the system. The river system contributes additional flow to the model. This can result in elevated higher heads in close proximity to the river. This system also becomes an additional drainage area added to the drain and GHB package. In further stress periods, the model with the river package will be used for paleo reconstruction.

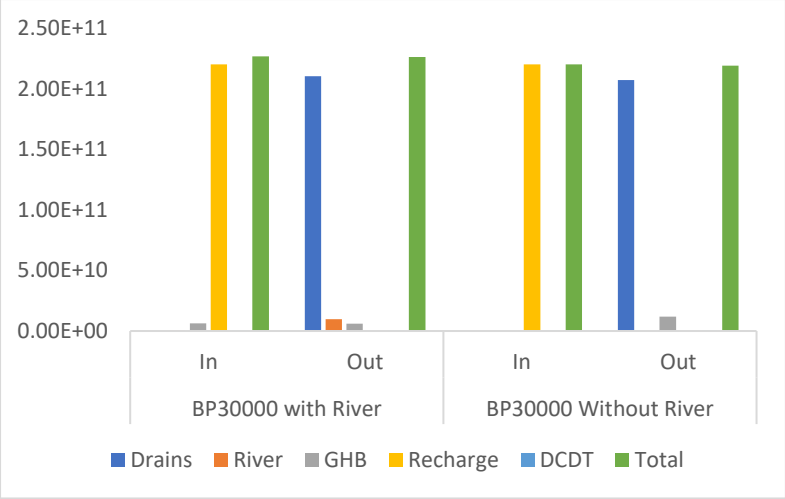

Figure 16. Water budget for a model with and without river

The water budget at different times in paleo reconstruction is illustrated in Figure xx. The displays in this graphic illustrate periods where significant differences in sea level. BP30000 is the starting point of paleo reconstruction with sea level around -110 m. From 29ka until 23ka most regression is happening in these periods, with BP23000 giving the lowest sea level in the paleo reconstruction. BP10000 is in the middle of the process of transgression with a sea level of around -15 m, followed by BP04000 and BP01000 coincide with the highest sea level and current sea level.

Most of the input comes from recharge, as this Island has quite a high precipitation rate. In addition to that, the low GHB conductance might influence the low input from GHB. The rate of recharge is gradually decreasing as the sea level rises, with the exception of the initial stress periods in paleo reconstruction. It is evident that when the sea level is at its highest, the recharge is reduced since there is less land available to receive the recharge. The output of the river system is higher when the sea level is higher contrary to output from GHB and drainage. Lower GHB output is due to increasing hydraulic gradient when sea level is increased while drainage output is lower due to decreasing drainage area due to the same reason (Figure 17). Higher river output might be to compensate for or replace some loss in the drainage area.

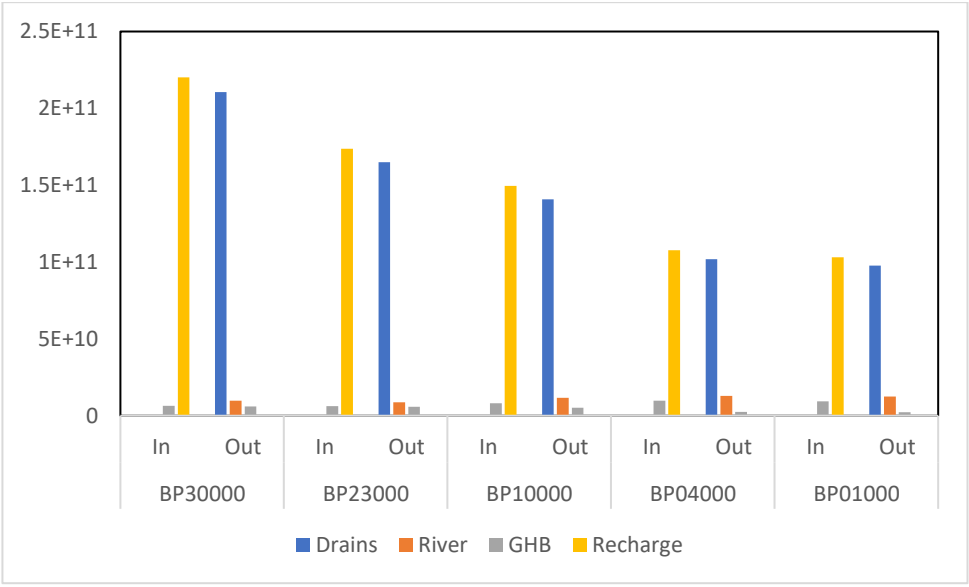

Figure 17. Water budget for Paleo reconstruction

One of the objectives of this initial salinity distribution for this paleo reconstruction is to identify the source and the formation of saline water in the inland areas. The studies by Prayogi et al. (2016), Putra et al. (2020), and Putranto & Rüde (2011) found some saline water in the inland areas quite far from the sea in Klaten, Semarang-Demak (Central Java), and Jakarta. The sources of the saline water in Klaten are strongly aligned with the fault zone in this area and trapped saline groundwater (Putra et al., 2016). While in Semarang-Demak and Jakarta, the potential sources of this saline water are due to pollution from agriculture and discharge from industrial areas (Prayogi et al., 2016; Putranto & Rude, 2011). These potential sources are not included in this model since it does not utilize local geology data (faults are not included) and does not incorporate anthropogenic causes of pollution. Thus, to illustrate the formation of saline water in inland areas is by making the impermeable layer (lowest layer) on the model has constant saline concentration throughout paleo reconstruction periods.

Several head profiles for some stress periods in paleo reconstruction are displayed in Figure 18 (in 3D) and Figure 19 (2D horizontal cross-section). The head gradient is increasing with the increase of sea level as evidenced by illustration in four stress periods below, BP30000 coincides with -110 m sea level, BP15000 with -98 m sea level, BP08000 with -10 m sea level, and BP01000 for current sea level condition. Most head profile has significant changes in the coastal areas as it directly affected by sea level rise. In the mountainous area, which is consistent above 500 msl, the head profile is relatively stable over time as the location is far away from the coastal area and only affected by recharge and river (well impact will incorporate in other scenarios).

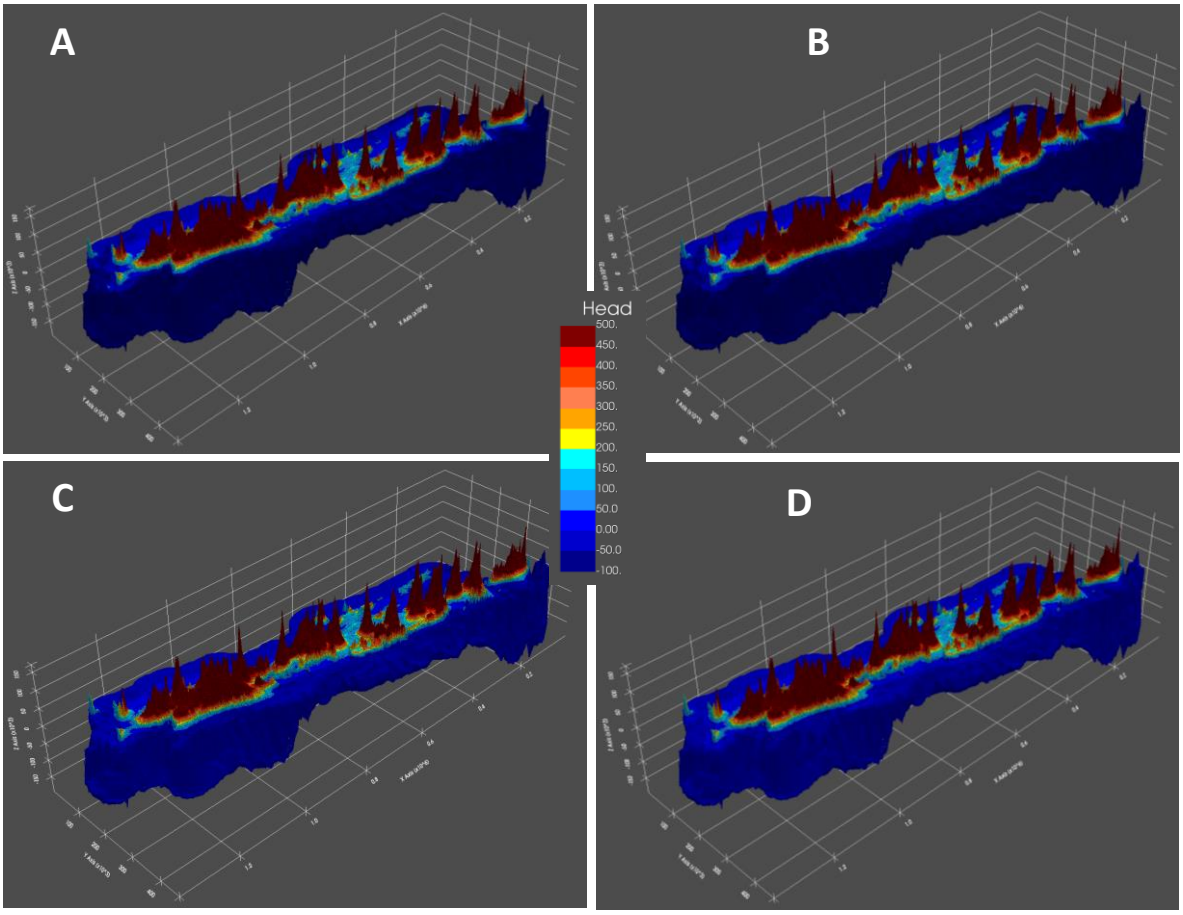

Figure 18. 3D Head Profile for BP30000 (A), BP15000 (B), BP08000(C), and BP01000 (D)

In Figure 19, the different head profiles between northern and southern coastal areas are more visible. The northern coast of Java is an area where the Java Sea is located with a relatively shallower sea depth compared to the southern coast area where the Indian Ocean is located. The head gradient is quite different between these two coastal areas. The head gradient is larger in southern coastal areas than in northern coastal areas as a result the surface elevation of the southern parts is steeper. In the northern regions, the surface elevation gradually decreases towards the coastal areas, which are characterized by alluvial and coastal plain morphology.

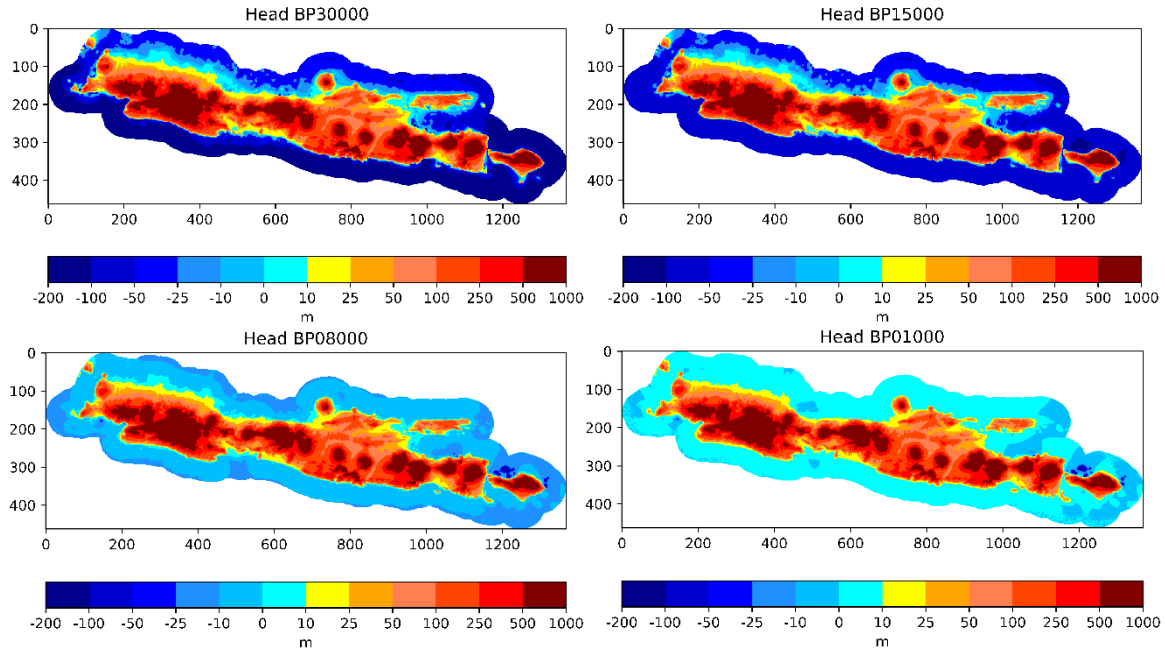

Figure 19. Head Profile for BP30000 (A), BP15000 (B), BP08000(C), and BP01000 (D)

Figure 20 and Figure 21 display the result of model concentrations in TDS. Throughout the entire reconstruction period, the model set the concentration in the area above sea level as freshwater, as depicted in Figure 20 below. Despite the homogenous conceptual geological layers, the transition thickness still can be investigated in Figure 21. As the sea level rises, the transition zone gets thinner, which can be seen in the south coastal area of Java Island (Figure 20 A-D) and the north coastal area (Figure 21 C-D).

The formation of saline water in inland areas can be seen in the cross-section of the model in Figure 21 (A-D). The upward movement of the saline water from the bottom layer of the model is due to the still quite permeable layer of the models and the thickness of the model. In the sedimentary rock layers, the hydraulic conductivity is set to be around 0.1 m/d. The process of dispersion of saline water from its initial salinity distribution to the state depicted in Figure 21 (B) requires approximately 10,000 years (all cross-sectional figures in the Appendix for further details). Figure 21 shows a horizontal cross-section that illustrates the presence of saline water in a thin layer surrounding mountainous regions. The flow of saline water is somewhat impeded by the aquitard in layer 6, however it eventually permeates through. The presence of high recharge zones in this region could have been a factor that impeded the spread of saline water in inland areas. This conceptual model demonstrates how saline water that was trapped during earlier geological periods can serve as a source of saline water in inland regions.

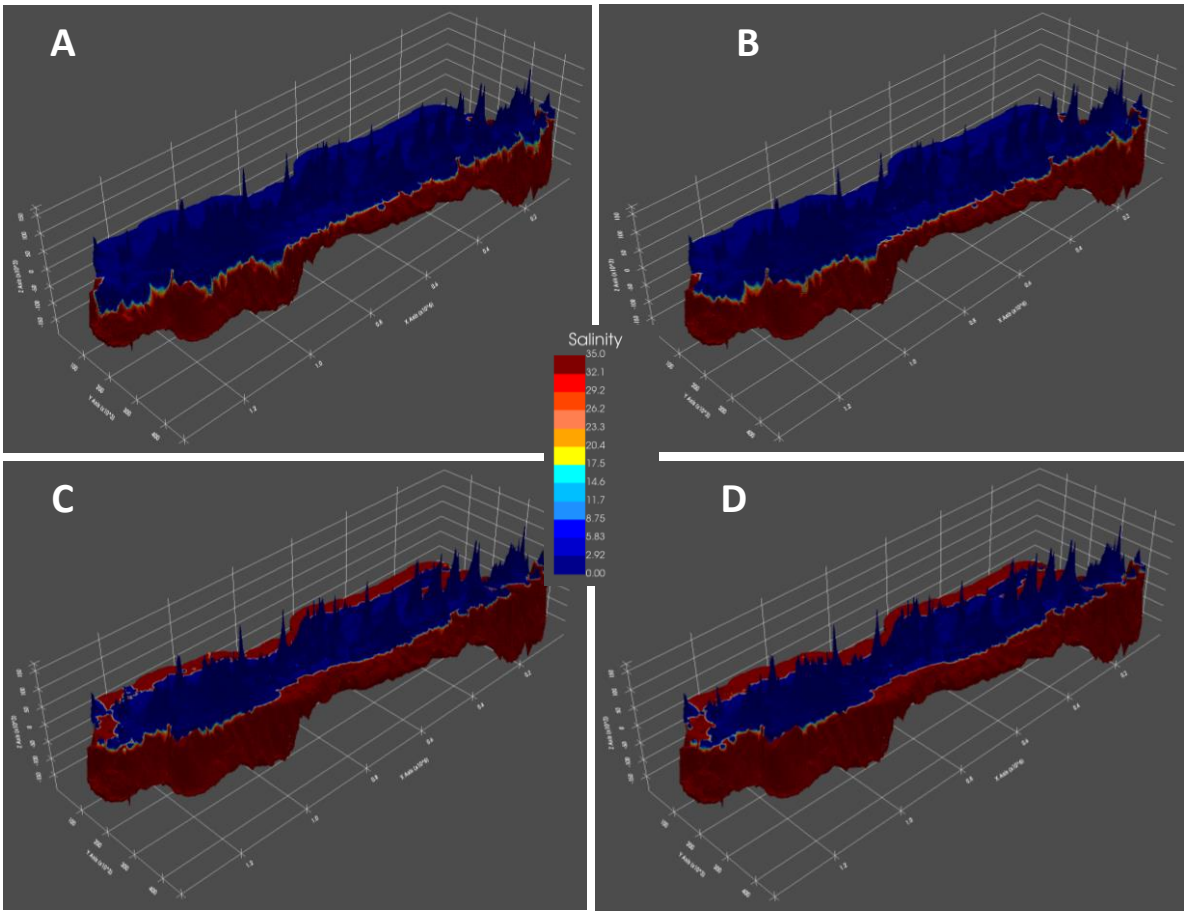

Figure 20. 3D Salinity Distribution for BP30000 (A), BP15000 (B), BP08000(C), and BP01000 (D)

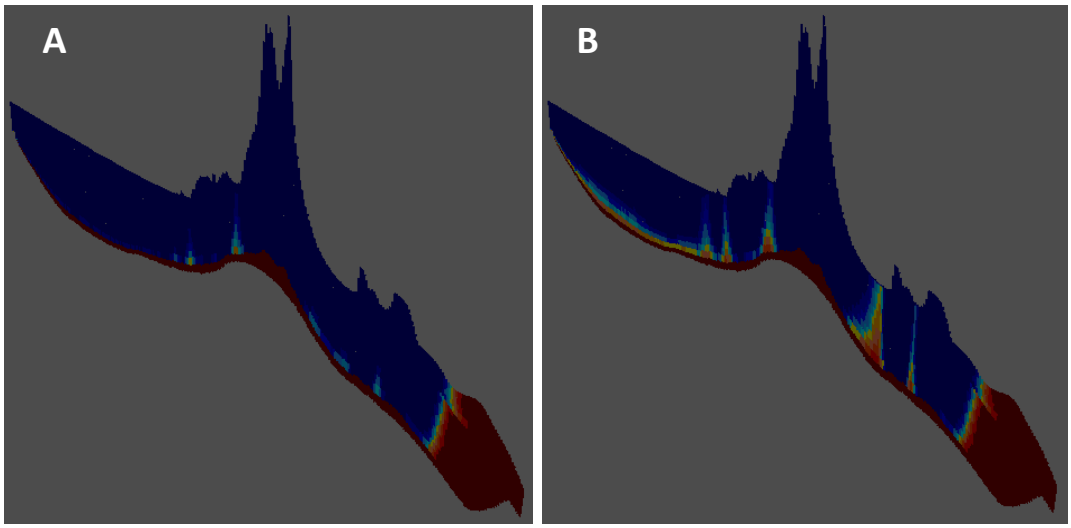

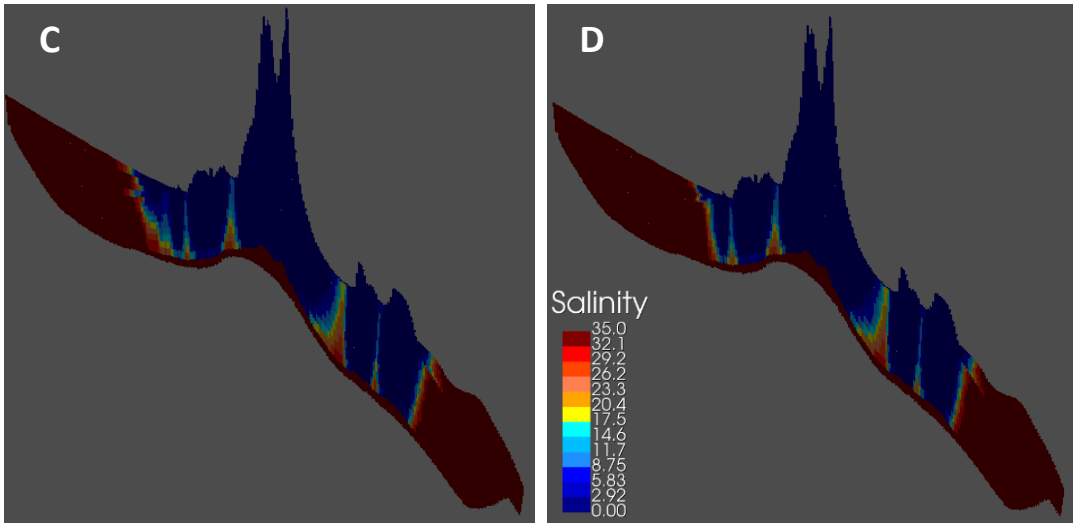

Figure 21. Salinity Distribution for BP30000 (A), BP15000 (B), BP08000(C), and BP01000 (D)

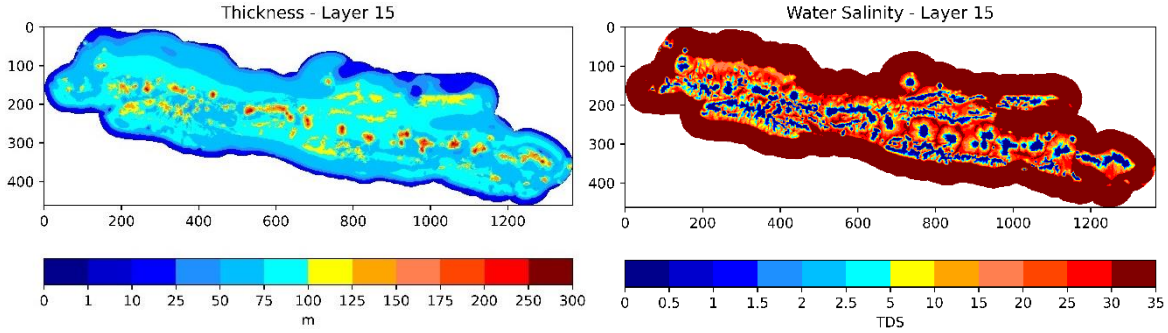

Figure 22. Thickness and modeled water salinity for layer 15 in BP01000.

The fluctuation of sea level is affecting the quantity of freshwater and solute mass during the paleo reconstruction period (Figure 23). The pattern of freshwater volume is decreasing, and solute mass is increasing as the sea level rises. A study by Van Engelen et al. (2019) showed a decrease in freshwater volume following sea level rise. There is a delay in the change of freshwater and solute mass after the sea level rises. In the first 15,000 years, the volume of freshwater did not have a significant change as the sea level in these periods didn't have big fluctuations.

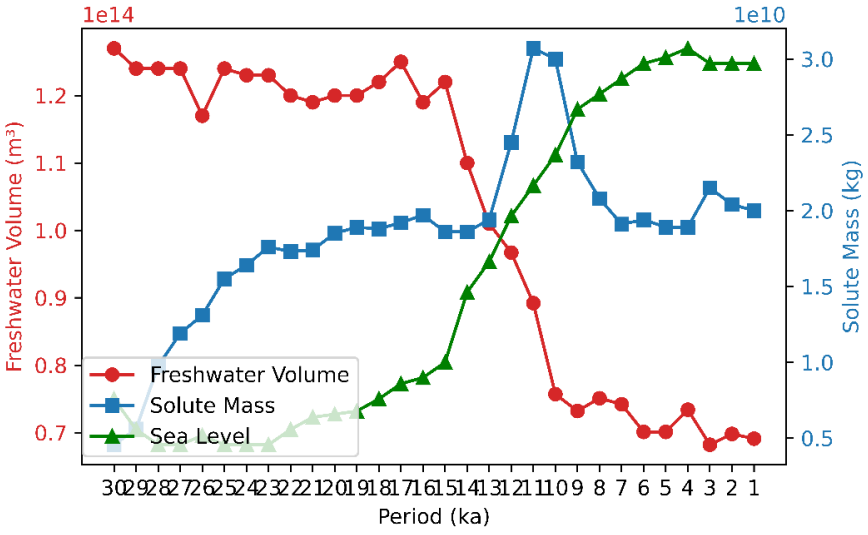

Figure 23. Freshwater volume and solute mass change over paleo reconstruction periods.

During the Holocene period, there was a substantial decrease in the amount of freshwater as a result of considerable fluctuations in sea level caused by periods of warming. In this era, there are significant shifts in solute mass. Approximately 13,000 years ago, there was a notable rise in the amount of solute mass following a large change in sea level approximately 15,000 years ago, followed by a sharp decline around 11,000 years ago. This phenomenon may be attributed to the gradual and steady rise in sea level following a large change in sea level and the onset of periods of freshening in the system. Following this decline, the solute mass exhibits a more stable fluctuation pattern.

3.4 Groundwater Abstraction Scenario

Two scenarios, which were groundwater abstraction and tidal inundation, were developed to illustrate the present condition of the Java Island coastal groundwater system. The salinity distribution and head profile for this model are based on the results obtained from the last stress periods in the paleo reconstruction (BP01000). The recharge and groundwater abstraction inputs using data from the PCR-GLOBWB model for the period between 1986 and 2015. This period was divided into three stress periods, SP_0 (1986-1995), SP_1 (1996-2005), and SP_2 (2006-2015). The units for recharge and groundwater abstraction are in m/day.

Figure 24 illustrates the water budget for three specific periods in the groundwater abstraction scenario, while Figure 25 provides a more detailed analysis of the quantity of groundwater extracted. The primary input for the model is recharge, which is followed by GHB. The recharge rate remains consistently stable during all three periods, with the last stress periods being characterized by a higher recharge rate. In the output, drains, and rivers become the main contributors to draining the water from the system. The impact of groundwater abstraction is not significant, as evidenced by the water budget. The amount of the groundwater extracted is increasing throughout stress periods (Figure 25).

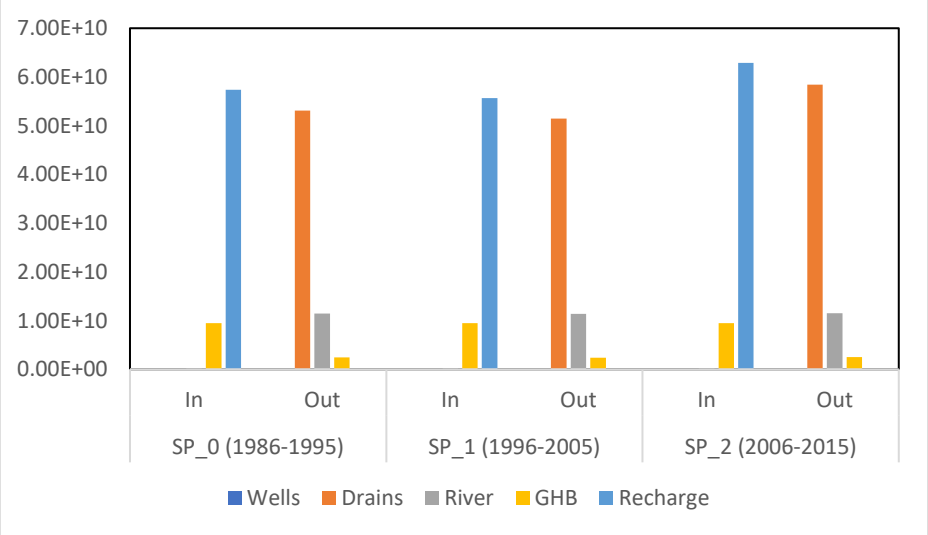

Figure 24. Water budget for groundwater abstraction scenario.

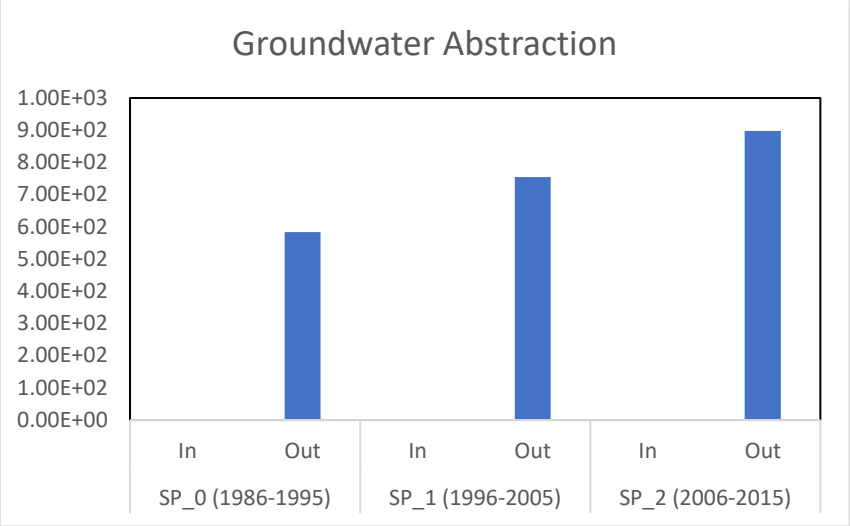

Figure 25. Volume of groundwater abstraction for three periods in the model

Figure 26 illustrates the decline of the groundwater table throughout three time periods in the model. The depletion of the groundwater table is determined by calculating the difference between the hydraulic head in the current model and the hydraulic head in the last stress period during the paleo reconstruction. Groundwater depletion is occurring primarily on the northern coast of Java Island. In the southern coast of Java, specifically in the region of Cilacap and Kebumen in Central Java, there has also been a significant decline in the groundwater table during these three periods. The majority of groundwater depletion is around 8 m.

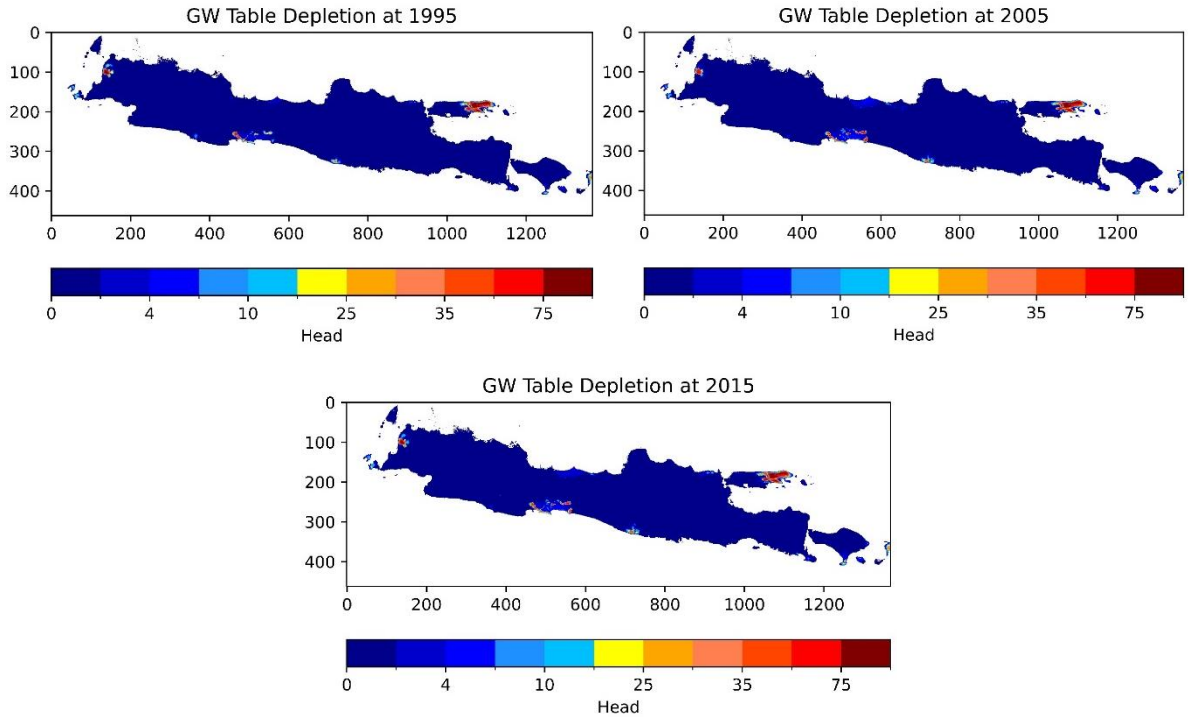

Figure 26. Groundwater table depletion for three different periods compared to the last stress period in paleo reconstruction.

In this scenario, it is strange that there is no indication of groundwater depletion in the Jakarta Region, despite this area having the greatest recorded groundwater abstraction according to the PCR-GLOBWB data. On the other side, on Madura Island, there is a substantial decrease in the groundwater table, with a drop of almost 75 meters. There may be a problem in implementing the

well package in the model. It is worth noting that the Jakarta area has a high recharge rate and can potentially receive infiltration from its catchment area surrounding Bogor which has a higher elevation.

3.5 Overwash Scenario

The last model for the present condition of groundwater status in Java is the overwash or tidal flooding scenario. Tidal flood is a recurring issue in Java Island, particularly in low-lying areas such as Pekalongan, Semarang, Demak, and Cilacap. Additionally, there are occurrences of tidal flooding in other regions along the North Coast of Java. However, in these areas, the frequency of floods is more frequent, and the resulting impact is significant.

The process of tidal inundation is not simulated in this study, instead, the possible outcome of this disaster is implemented as the initial head and salinity distribution. This scenario is based on a study by Oude Essink et al. (2014) by adapting Henry's concept in order to demonstrate the influence of a tsunami on a coastal aquifer system. The temporary sea level for tidal flooding is approximately rising around 1.5-2 m, based on the worst record of tidal flooding in the Semarang-Demak areas. Furthermore, for the initial salinity distribution, the coastal areas with a surface elevation of less than 2 m have saline water concentration (only on the first layer) as a result of days of tidal flooding. The impact of this event is investigated for 100 years further which is divided for every 20 years (one stress period).

After the tidal flooding, the solute mass is sharply increased as can be seen in Figure 27. The first bar graph is the solute mass in the lass stress period of groundwater abstraction scenario which the salinity distribution is modified as the initial salinity distribution for this scenario. The solute mass gradually decreased over time (Figure xx). After a century, the mass of solute has not returned to its initial distribution of salinity, which can have an influence on the supply of groundwater due to decreased groundwater quality.

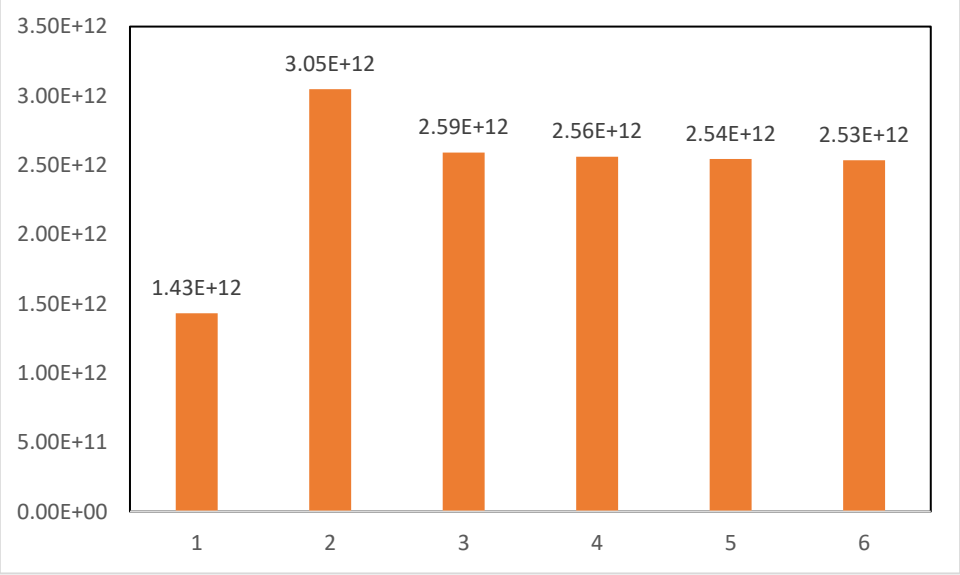

Figure 27. Solute mass changes every 20 years after tidal inundation.

Figure 28 displays the first layer of horizontal cross-section of the salinity distribution in the overwash scenario at the beginning of the event and 20 and 40 years after the tidal flooding incident. The region most impacted by tidal floods encompasses the entire northern coast of Java and the southern coastal area of Central Java. This region is characterized by a relatively low elevation,

making it more susceptible to this particular threat (Willemsen et al., 2019). At the beginning of the flood, the coastal region with a surface elevation lower than 2 m has salt water due to seawater that moves to inland areas. After 20 years, the inland regions are slowly becoming fresh again as can be seen in the north coast areas. There are still some areas with higher saline concentrations like on the north coast of East Java and near Jakarta areas. Moderately saline concentrations are still found in Semarang-Demak areas in Central Java.

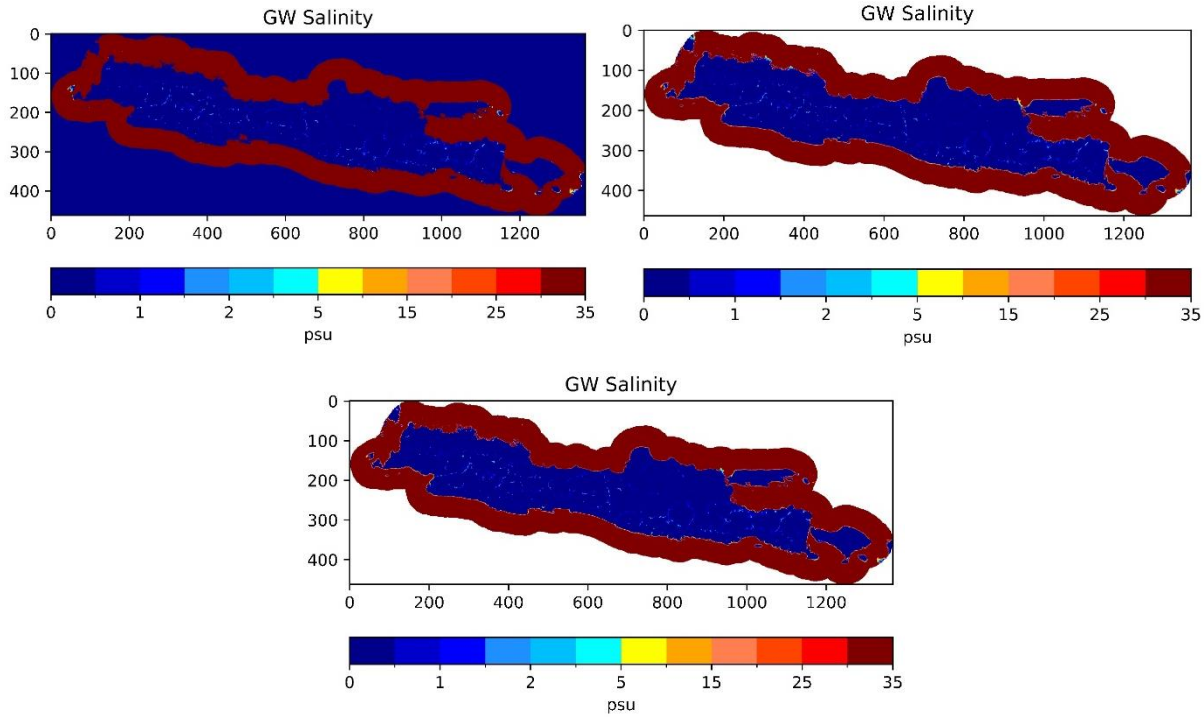

Figure 28. Horizontal cross-section for change in salinity distribution.

3.6 Observed Salinity and Model Salinity

This model employed global data and exclusively relied on conceptual hydrogeological structures for the layers within the model. Therefore, it was anticipated that the model's performance would not accurately reflect the field condition of the Java groundwater system due to its complicated hydrogeological structure.

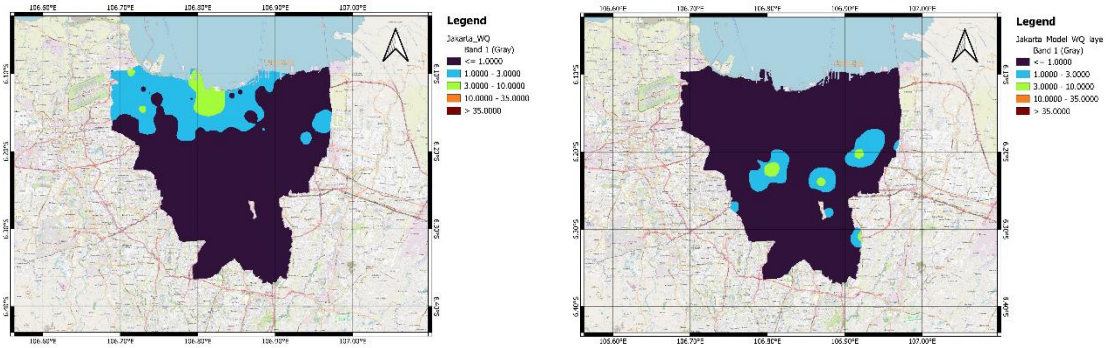

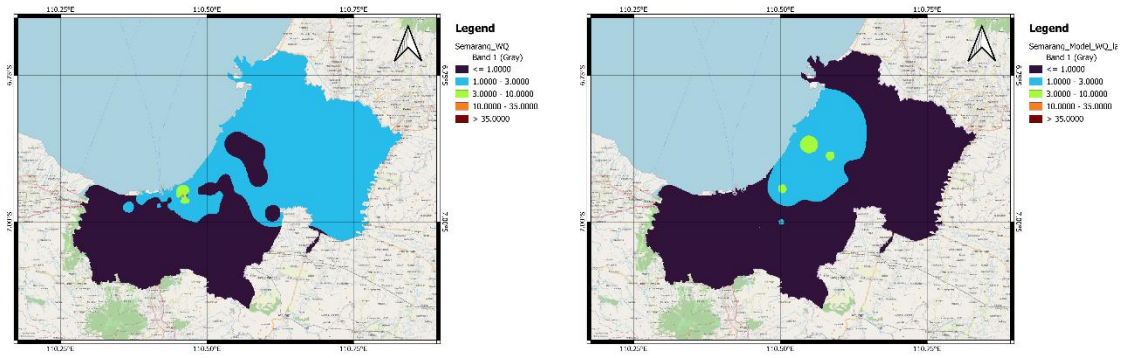

Figure 29. Water salinity distribution for Jakarta and Semarang-Demak (left = interpolation from observation data; right = model result).

The interpolation of groundwater salinity in unit TDS in Jakarta and Semarang-Demak areas is shown on the left side of Figure 29. The right side displays the output of the model's salinity in layer 5, which approximately matches the depth of the well observation at around 40-60 meters below sea level.

The salinity category is divided into five classes based on USGS classification (chapter 2). Overall, the model did well in demonstrating the area with freshwater concentration (below 1 g/l TDS). In the Jakarta area, the model's representation of salinity did not accurately reflect the observed distribution of salinity, particularly in the coastline regions. The depth of the saline-freshwater interface in the model appears to be greater below layer 5. The presence of inland salinity in the model's salinity distribution is attributed to the constant concentration of saltwater in the last layer of the model. In the Semarang-Demak areas, the model salinity has better performance than in the Jakarta area. In the model salinity, there is slightly saline water represented corresponding to the observed salinity. The performance of this model could be better by including the local geological data, so the salinity and head distribution could better represent the field condition.

4. Conclusions and Recommendations

This study has the main objective to simulate the Coastal Java groundwater system using a 3D global coastal groundwater model (GCGM) developed by Deltares and Utrecht University. In this internship, three model scenarios are conducted which are paleo reconstruction, groundwater abstraction, and tidal flooding scenarios.

Before going into scenarios, models with various DT0 values were made. The DT0 parameter could speed up the computation running time of the model. It was found that the difference in salinity and head distribution of these several models is not high. The majority of the difference is still below 10%. Thus, in the later scenarios, a high DT0 value was chosen to speed up the model run.

The paleo reconstruction was developed using two different initial salinity distribution scenarios. The result of this different scenario is only on the formation of inland salinity in the second model which wants to identify the possible source of salinity in the inland areas. Over time the volume of freshwater is declining due to sea level rise and vice versa for solute mass. In this model, the river package was added to the model due to the importance of surface-groundwater interaction in the Java groundwater system.

The represent current scenario, two scenarios were made which are groundwater abstraction and tidal flooding scenarios. The groundwater abstraction scenarios showed the vulnerability of the northern coast areas due to groundwater abstraction although the strange result for the Jakarta areas. The tidal flooding scenario showed the long-lasting impact of temporal time of sea level rise due to tidal floods. After 100 years, there are still some areas in the coastal zone that have quite saline water concentrations in their groundwater system. Last, the model salinity is doing well in representing the areas with freshwater concentrations but could be better for the areas with saline water concentration by including the local geological data.

5. References

Alkurd, M. M. F. (2023). *Paleo-hydrogeographical model for the Levant applying 3D supra-regional coastal groundwater modelling approach*.

Andreadis, K. M., Schumann, G. J. P., & Pavelsky, T. (2013). A simple global river bankfull width and depth database. *Water Resources Research*, *49*(10), 7164–7168. https://doi.org/10.1002/wrcr.20440

Andreas, H., Usriyah, Zainal Abidin, H., & Anggreni Sarsito, D. (2017). Tidal inundation ("Rob") investigation using time series of high resolution satellite image data and from institu measurements along northern coast of Java (Pantura). *IOP Conference Series: Earth and Environmental Science*, *71*(1). https://doi.org/10.1088/1755-1315/71/1/012005

Asian Development Bank. (2016). *Indonesia Country Water Assessment*. ASIAN DEVELOPMENT BANK. https://www.adb.org/sites/default/files/institutional-document/183339/ino-water-assessment.pdf

Badan Pusat Statistik. (2023). *Statistik Indonesia 2023*. https://www.bps.go.id/publication/2023/02/28/18018f9896f09f03580a614b/statistik-indonesia-2023.html

Beyer, R. M., Krapp, M., & Manica, A. (2020). High-resolution terrestrial climate, bioclimate and vegetation for the last 120,000 years. *Scientific Data*, *7*(1). https://doi.org/10.1038/s41597-020-0552-1

Bott, L. M., Schöne, T., Illigner, J., Haghshenas Haghighi, M., Gisevius, K., & Braun, B. (2021). Land subsidence in Jakarta and Semarang Bay – The relationship between physical processes, risk perception, and household adaptation. *Ocean and Coastal Management*, *211*. https://doi.org/10.1016/j.ocecoaman.2021.105775

Handayani, W., & Kumalasari, N. R. (2015). Migration as Future Adaptive Capacity: The Case of Java — Indonesia. In *Environmental Change, Adaptation and Migration* (pp. 117–138). Palgrave Macmillan UK. https://doi.org/10.1057/9781137538918_7

Horspool, N., Pranantyo, I., Griffin, J., Latief, H., Natawidjaja, D. H., Kongko, W., Cipta, A., Bustaman, B., Anugrah, S. D., & Thio, H. K. (2014). A probabilistic tsunami hazard assessment for Indonesia. *Natural Hazards and Earth System Sciences*, *14*(11), 3105–3122. https://doi.org/10.5194/nhess-14-3105-2014

Intergovernmental Panel on Climate Change (IPCC). (2022). Sea Level Rise and Implications for Low-Lying Islands, Coasts and Communities. In *The Ocean and Cryosphere in a Changing Climate* (pp. 321–446). Cambridge University Press. https://doi.org/10.1017/9781009157964.006

Irawan, D. E., Silaen, H., Sumintadireja, P., Lubis, R. F., Brahmantyo, B., & Puradimaja, D. J. (2015). Groundwater–surface water interactions of Ciliwung River streams, segment Bogor–Jakarta, Indonesia. *Environmental Earth Sciences*, *73*(3), 1295–1302. https://doi.org/10.1007/s12665-014-3482-4

Kim, H. L., Li, T., Kalsi, N., Nguyen, H. T. T., Shaw, T. A., Ang, K. C., Cheng, K. C., Ratan, A., Peltier, W. R., Samanta, D., Pratapneni, M., Schuster, S. C., & Horton, B. P. (2023). Prehistoric human migration between Sundaland and South Asia was driven by sea-level rise. *Communications Biology*, *6*(1). https://doi.org/10.1038/s42003-023-04510-0

Mulder, T. (2018). *Constructing 3D variable-density groundwater flow models for six deltas using global data sets*.

Oude Essink, G., Faneca Sànchez, M., & Zamrsky, D. (2014). Global Quick Scan of the Vulnerability of Groundwater systems to Tsunamis. In *Geophysical Research Abstracts* (Vol. 16).

Pelletier, J. D., Broxton, P. D., Hazenberg, P., Zeng, X., Troch, P. A., Niu, G. Y., Williams, Z., Brunke, M. A., & Gochis, D. (2016). A gridded global data set of soil, intact regolith, and sedimentary deposit thicknesses for regional and global land surface modeling. *Journal of Advances in Modeling Earth Systems*, *8*(1), 41–65. https://doi.org/10.1002/2015MS000526

Prayogi, T. E., Abdillah, F., Mora Nasution, E., Janner,), Nababan, R., Mochamad,), Memed, W., Daryanto, A., Konservasi, B., Tanah, A., Geologi, B., Energi, K., Sumber, D., & Mineral, D. (2016). *Penilaian kualitas air tanah pada akuifer tidak tertekan untuk keperluan air minum di wilayah utara Cekungan Air Tanah Jakarta Groundwater Quality Assesment of Unconfined Aquifer System for Suitable Drinking Determination at Northern Jakarta Groundwater Basin*.

Purnama, S., & Marfai, M. A. (2011). SALINE WATER POLLUTION IN GROUNDWATER: ISSUES AND ITS CONTROL. *Journal of Natural Resources and Development*. https://doi.org/10.5027/jnrd.v2i0.06

Putra, D. P. E., Halim, D., Widagdo, S. S., & Surya Atmaja, R. R. (2020). Degradation of groundwater quality due to the occurrence of salty-tasted water in Bayat District, Klaten, Central Java, Indonesia. *Journal of Degraded and Mining Lands Management*, *8*(1), 2525–2536. https://doi.org/10.15243/JDMLM.2020.081.2525

Putranto, T. T., & Rüde T R. (2011). *HYDROGEOLOGY OF SEMARANG DEMAK GROUNDWATER BASIN: AN OVERVIEW AND ITS CHALLENGES IN PRELIMINARY GROUNDWATER FLOW MODELING*.

Putranto, T. T., & Rüde, T. R. (2016). Hydrogeological model of an urban city in a coastal area, case study: Semarang, Indonesia. *Indonesian Journal on Geoscience*, *3*(1), 17–27. https://doi.org/10.17014/ijog.3.1.17-27

Sathiamurthy, E., & Voris, H. K. (2006). Maps of Holocene Sea Level Transgression and Submerged Lakes on the Sunda Shelf. In *The Natural History Journal of Chulalongkorn University, Supplement* (Vol. 2). http://www.ngdc.-

Supendi, P., Widiyantoro, S., Rawlinson, N., Yatimantoro, T., Muhari, A., Hanifa, N. R., Gunawan, E., Shiddiqi, H. A., Imran, I., Anugrah, S. D., Daryono, D., Prayitno, B. S., Adi, S. P., Karnawati, D., Faizal, L., & Damanik, R. (2023). On the potential for megathrust earthquakes and tsunamis off the southern coast of West Java and southeast Sumatra, Indonesia. *Natural Hazards*, *116*(1), 1315–1328. https://doi.org/10.1007/s11069-022-05696-y

Sutanudjaja, E. H., Van Beek, R., Wanders, N., Wada, Y., Bosmans, J. H. C., Drost, N., Van Der Ent, R. J., De Graaf, I. E. M., Hoch, J. M., De Jong, K., Karssenberg, D., López López, P., Peßenteiner, S., Schmitz, O., Straatsma, M. W., Vannametee, E., Wisser, D., & Bierkens, M. F. P. (2018). PCR-GLOBWB 2: A 5 arcmin global hydrological and water resources model. *Geoscientific Model Development*, *11*(6), 2429–2453. https://doi.org/10.5194/gmd-11-2429-2018

USAID. (2021). *Indonesia Water Resources Profile Overview*. https://www.globalwaters.org/resources/assets/indonesia-water-resources-profile

Van Engelen, J., Verkaik, J., King, J., Nofal, E. R., Bierkens, M. F. P., & Oude Essink, G. H. P. (2019). A three-dimensional palaeohydrogeological reconstruction of the groundwater salinity

distribution in the Nile Delta Aquifer. *Hydrology and Earth System Sciences*, *23*(12), 5175–5198. https://doi.org/10.5194/hess-23-5175-2019

Verkaik, J., van Engelen, J., Huizer, S., Bierkens, M. F. P., Lin, H. X., & Oude Essink, G. H. P. (2021). Distributed memory parallel computing of three-dimensional variable-density groundwater flow and salt transport. *Advances in Water Resources*, *154*. https://doi.org/10.1016/j.advwatres.2021.103976

Weatherall, P., Marks, K. M., Jakobsson, M., Schmitt, T., Tani, S., Arndt, J. E., Rovere, M., Chayes, D., Ferrini, V., & Wigley, R. (2015). A new digital bathymetric model of the world's oceans. *Earth and Space Science*, *2*(8), 331–345. https://doi.org/10.1002/2015EA000107

Widodo, J., Herlambang, A., Sulaiman, A., Razi, P., Yohandri, Perissin, D., Kuze, H., & Sri Sumantyo, J. T. (2019). Land subsidence rate analysis of Jakarta Metropolitan Region based on D-InSAR processing of Sentinel data C-Band frequency. *Journal of Physics: Conference Series*, *1185*, 012004. https://doi.org/10.1088/1742-6596/1185/1/012004

Willemsen, P., van der Lelij, A. C., & van Wesenbeeck, B. (2019). *Vulnerability Assessment North Coast Java*. https://www.ecoshape.org/app/uploads/sites/2/2020/02/1220476-002-ZKS-0007_v0.1-Risk-Assessment-North-Coast-Java-final.pdf

Zamrsky, D., Oude Essink, G. H. P., & Bierkens, M. F. P. (2018). Estimating the thickness of unconsolidated coastal aquifers along the global coastline. *Earth System Science Data*, *10*(3), 1591–1603. https://doi.org/10.5194/essd-10-1591-2018

Appendix

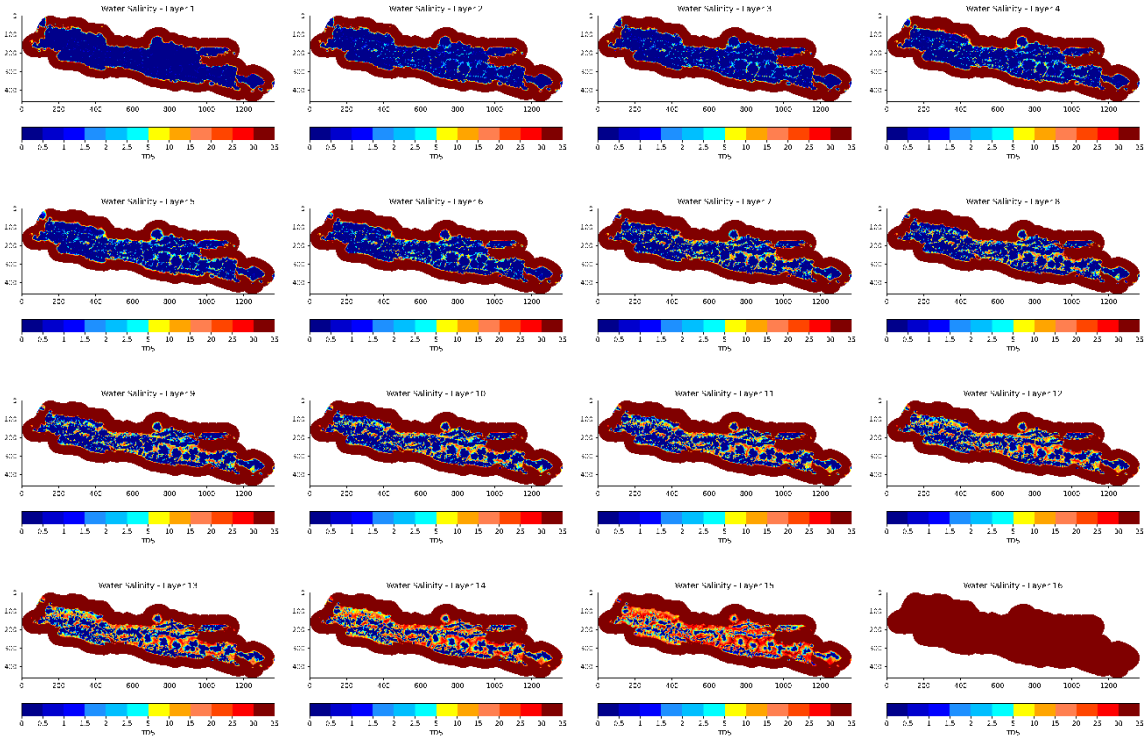

Figure A1. Salinity distribution for every layer

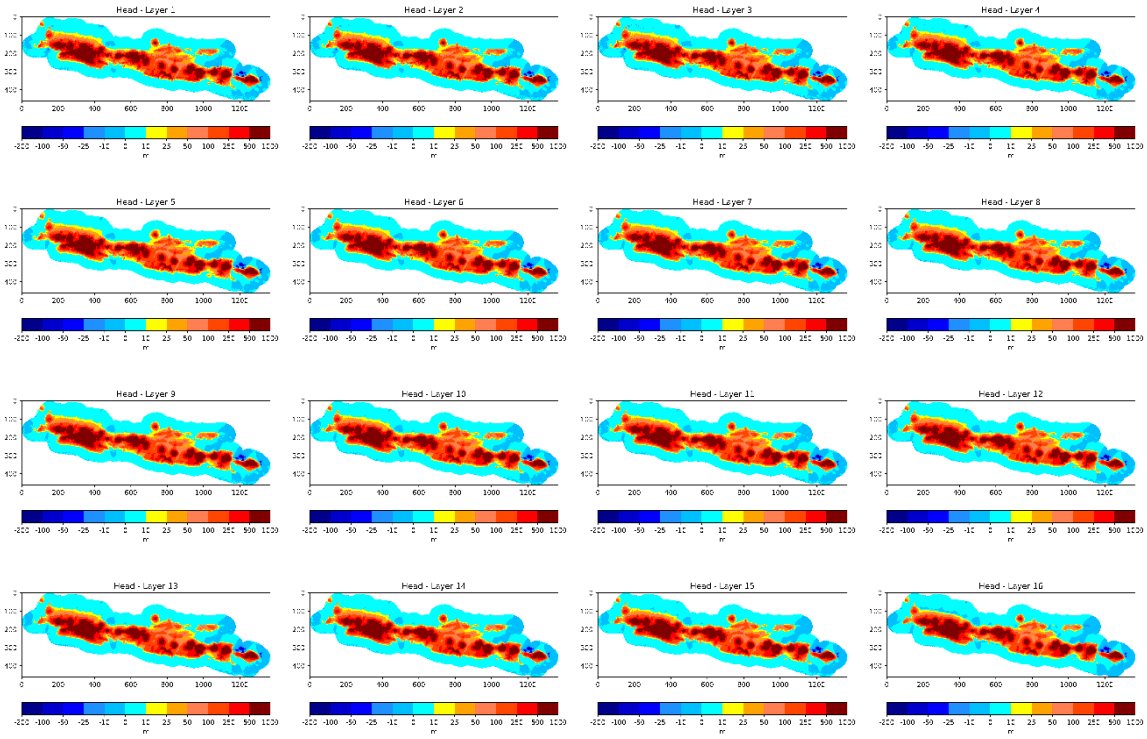

Figure A2. Head profile for every layer

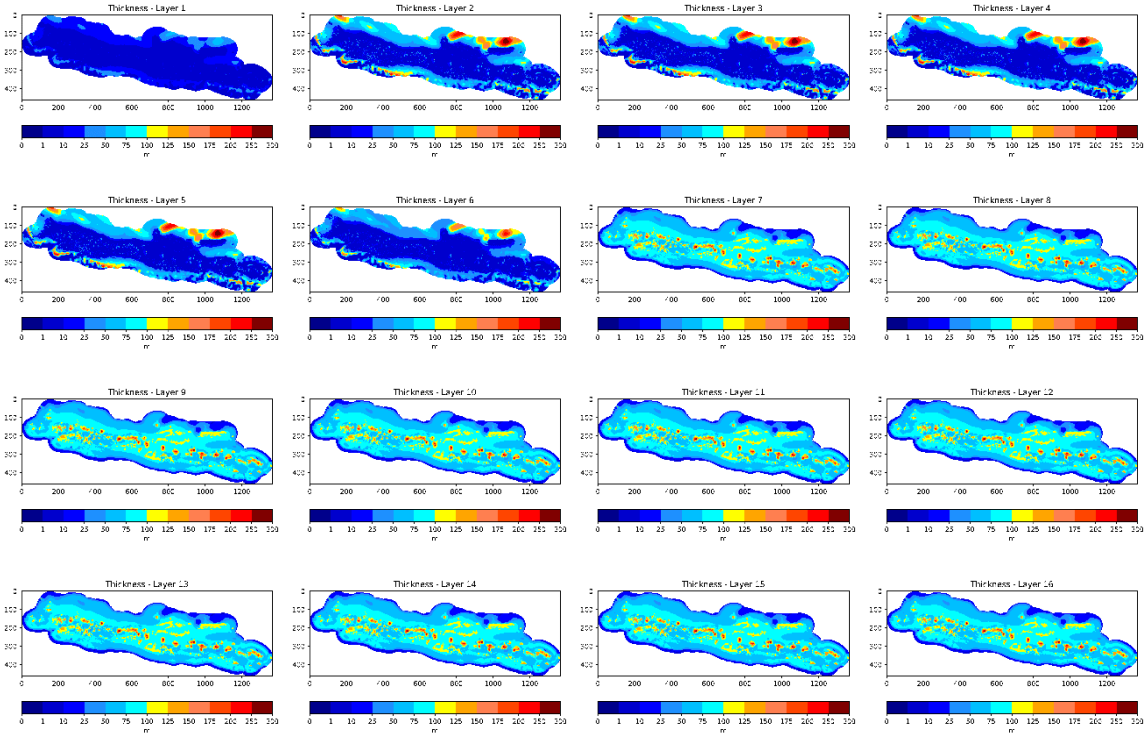

Figure A3. Thickness for every layer